Diagenesis of Hunton Group Carbonates (Silurian) West Carney Field, Logan and Lincoln Counties, Oklahoma, U.S.A.

Cesar Silva[1], Brian J. Smith[2], Jordan T. Ray[3], James R. Derby[4], and Jay M. Gregg[5, 6]
[1]*Hocol, Bogotá, Bogotá D.C. Department, Colombia casilvacar@yahoo.es*
[2]*Continental Resources, Oklahoma City, OK, 73102 U.S.A. smit1647@live.com*
[3]*Boone Pickens School of Geology, Oklahoma State University, Stillwater, OK 74078 U.S.A. jtray.geo@gmail.com*
[4]*Independent Geologist, Leonard, OK, 74043 jderby@olp.net*
[5]*Boone Pickens School of Geology, Oklahoma State University, Stillwater, OK, 74078 U.S.A. jay.gregg@okstate.edu*
[6]*Corresponding author*

ABSTRACT

The West Carney Hunton Field (WCHF) is an important oil field in central Oklahoma. Deposited during a series of sea-level rises and falls on a shallow shelf, the Cochrane and Clarita Formations (Hunton Group) have undergone a complex series of diagenetic events. The Hunton section of the WCHF comprises dolomitized crinoidal packstones, brachiopod "reefs" and grainstones, thin intervals of fine-grained crinoidal wackestones, and infrequent mudstones that were diagenetically affected by repeated sea-level change. Widespread karst is evidenced by multiple generations of solution-enlarged fractures, vugs, and breccias, which extend through the entire thickness of the Hunton. Karst development likely occurred during sea-level lowstands. Partial to complete dolomitization of Hunton limestones is interpreted to have occurred as a result of convective circulation of normal seawater during sea-level highstands. Open-space-filling calcite cements postdate dolomitization and predate deposition of the overlying siliciclastic section, which comprises the Misener Sandstone and Woodford Shale. Petrographic evaluation and carbon and oxygen isotope values of the calcite cements suggest precipitation by Silurian seawater and mixed seawater and meteoric water. Carbon and oxygen isotopic signatures of dolomite may have been partially reset by dedolomitization that was concurrent with calcite cementation. Fluid inclusions in late diagenetic celestite crystals observed in the Clarita Formation indicate that the WCHF was invaded by saline basinal fluids and petroleum after burial, during later stages of diagenesis. The timing of late diagenetic fluid flow and petroleum generation likely was during the Ouachita orogeny, which was occurring to the south. There is no evidence that late diagenetic fluids significantly altered the dolomite reservoir that formed earlier. The WCHF provides an ancient example of early diagenetic dolomitization by seawater that remains relatively unaltered by later diagenetic events.

Midcontinent Geoscience • Volume 1 • September 2020

Midcontinent Geoscience is an open-access, peer-reviewed journal of the Kansas Geological Survey. The journal publishes original research on a broad array of geoscience topics, with an emphasis on the midcontinent region of the United States, including the Great Plains and Central Lowland provinces.

INTRODUCTION

The West Carney Hunton Field (WCHF) is located in central Oklahoma in Lincoln and Logan Counties (T. 15 N., R. 1 and 2 E.) (fig. 1a, b). Situated on the Cherokee Platform directly east of the Nemaha Uplift (fig. 2), the WCHF covers nearly 121.4 km^2 (30,000 acres). The field consists of a shallow water carbonate reservoir with more than 250 producing wells. The WCHF produces out of the Chimneyhill Subgroup of the Hunton Group (Silurian) (fig. 3), which is a major producing horizon across much of Oklahoma (Derby et al., 2002a, 2002b). The sedimentology and stratigraphy of the Hunton Group in Lincoln and Logan counties are relatively well understood (Derby et al., 2002a, 2002b; Derby, 2007; Bader et al., 2007; Bader, 2007; Braimoh, 2010). Conodont biostratigraphy of the study area was extensively studied by Barrick (unpublished report; see Bader et al., 2007, and Derby, 2007). Little is known, however, about the diagenetic processes that affected the reservoir.

Using petrographical, geochemical, and mineralogical data, this study investigates the early and late diagenetic processes that affected the WCHF, with particular emphasis on dolomitization of the limestones. Collectively, these data are consistent with a model of shallow burial dolomitization by normal seawater that is largely unaltered by late diagenetic basinal fluids. This study, therefore, has implications for the origin of other Silurian dolomite reservoirs in the region as well as the origin of ancient dolomites in general.

GEOLOGICAL SETTING

During the Llandoverian (Early Silurian Period), warm, equatorial seawater favored the deposition of carbonates in Laurentia, northeastern Avalonia, Baltica, Siberia, and equatorial Gondwana (Scotese and McKerrow, 1990). A shallow epicontinental sea covered most of the continent of Laurentia (Scotese, 2002), which was a restricted basin under arid conditions (Derby, 2007). Sea-level changes affected carbonate deposition in the WCHF study area during this time with five major highstands during the Lower Silurian and three during the Upper Silurian (Johnson, 2006) (fig. 3).

The Oklahoma Basin was the major depocenter in Oklahoma and northern Texas during the Early to Middle Paleozoic Era (Johnson, 1987). Strata in most parts of the Oklahoma Basin are widespread and laterally persistent. The rise of the Nemaha Uplift and Ouachita Mountains during the Pennsylvanian split the Oklahoma Basin into the Anadarko Basin and Southern Oklahoma Aulacogen to the west and southwest and the Arkoma Basin to the

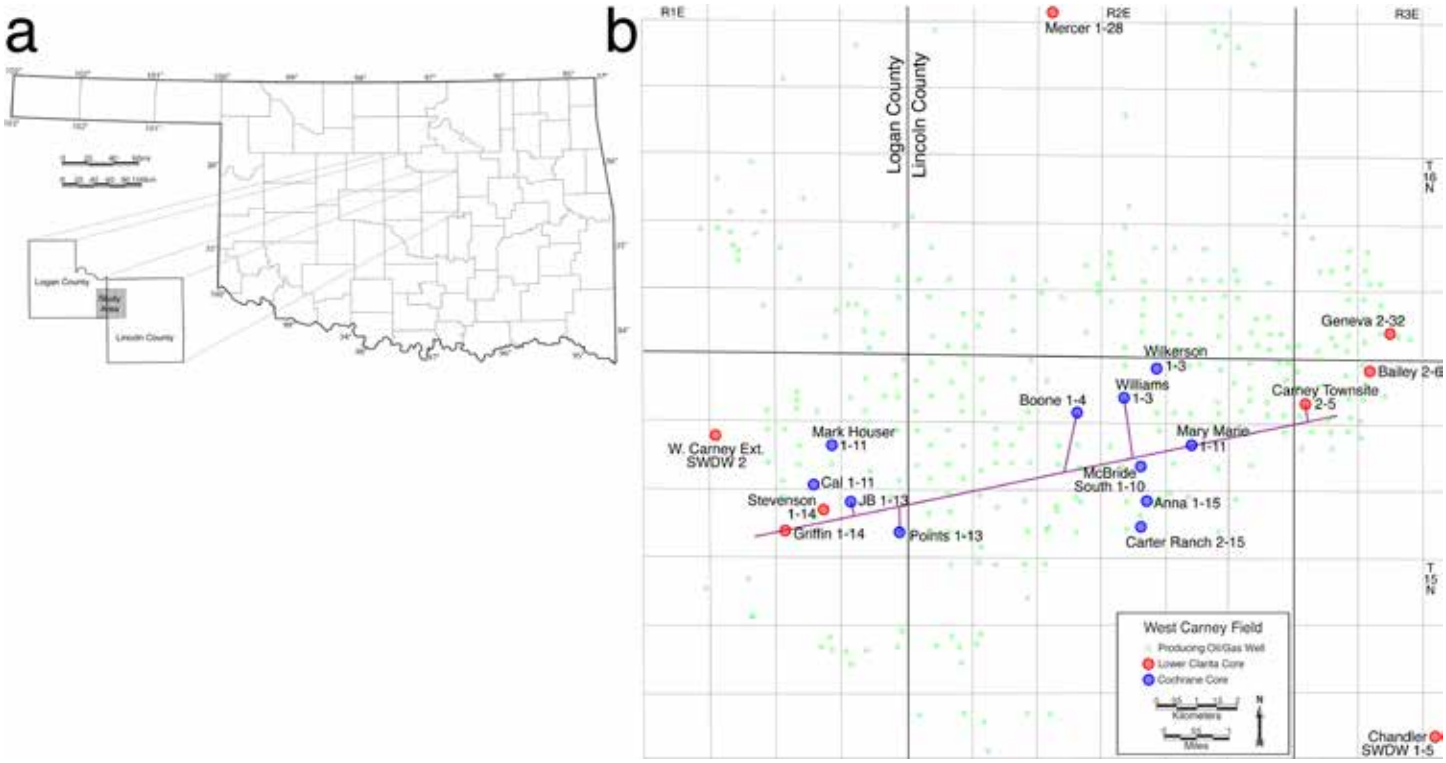

Figure 1. (a) Location of the WCHF study area. (b) Oil well and core locations in the WCHF. The line of the section shown in fig. 4 is indicated.

southeast. The WCHF study area is located on the western side of the Cherokee Platform (fig. 2). During the early Paleozoic Era, the depositional slope of the Oklahoma Basin was southwestward into the Southern Oklahoma Aulacogen (Derby et al., 2002a). Later development of the Nemaha Uplift to the west and tectonic subsidence in the Arkoma Basin to the southeast tilted the study area eastward. This eastward tilting continued throughout the late Paleozoic. The study area was subsequently tilted southwestward during the Mesozoic Era, resulting in the modern structural dip of about 8.5 m per km toward the southwest (Derby et al., 2002a).

The Hunton Group was deposited in a broad, mostly shallow epicontinental sea, with the depositional slope trending southwestward into the more subsiding part of the Anadarko Basin (Derby et al., 2002a). The Chimneyhill Subgroup is the only stratigraphic unit of the Hunton mapped in the WCHF. Regionally, the Chimneyhill Subgroup comprises (from oldest to youngest) the Keel, Cochrane, and Clarita Formations, with the Keel Formation being locally absent in the study area (fig. 3 and 4).

The thickness of the Hunton Group ranges from 7 to 42 m (24 to 139 ft) in the study area. The shallow marine carbonates of the Chimneyhill Subgroup are the major petroleum reservoir (Derby et al., 2002b). Derby (2007) recognized five "megafacies" within the Chimneyhill Subgroup: (1) reef and reef flank, (2) brachiopod biostrome, (3) lagoonal, (4) dolomitized shoalwater grainstone, and (5) deep water. The carbonates are unconformably overlain by the Late Devonian Misener Sandstone Member (which is only a few cm thick in the study area) and Late Devonian to Early Mississippian Woodford Shale. The Hunton is underlain in the study area by the Late Ordovician Sylvan Shale.

Derby (2007) and Braimoh (2010), using conodont data of Barrick (unpublished report), subdivided the Cochrane Formation into three informal units: the lower Cochrane member, the upper Cochrane A member, and

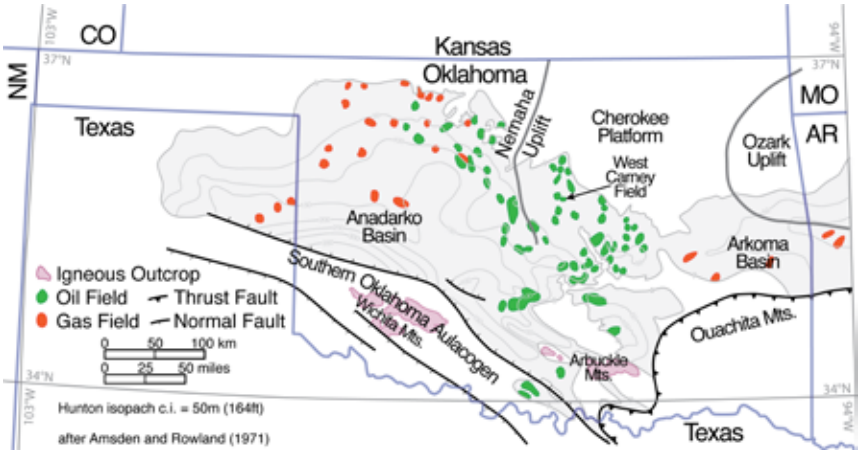

Figure 2. Isopach map showing Hunton Group thickness and Hunton Group oil and gas reservoirs in Oklahoma and western Arkansas. Major tectonic features also are shown (after Amsden and Rowland, 1971).

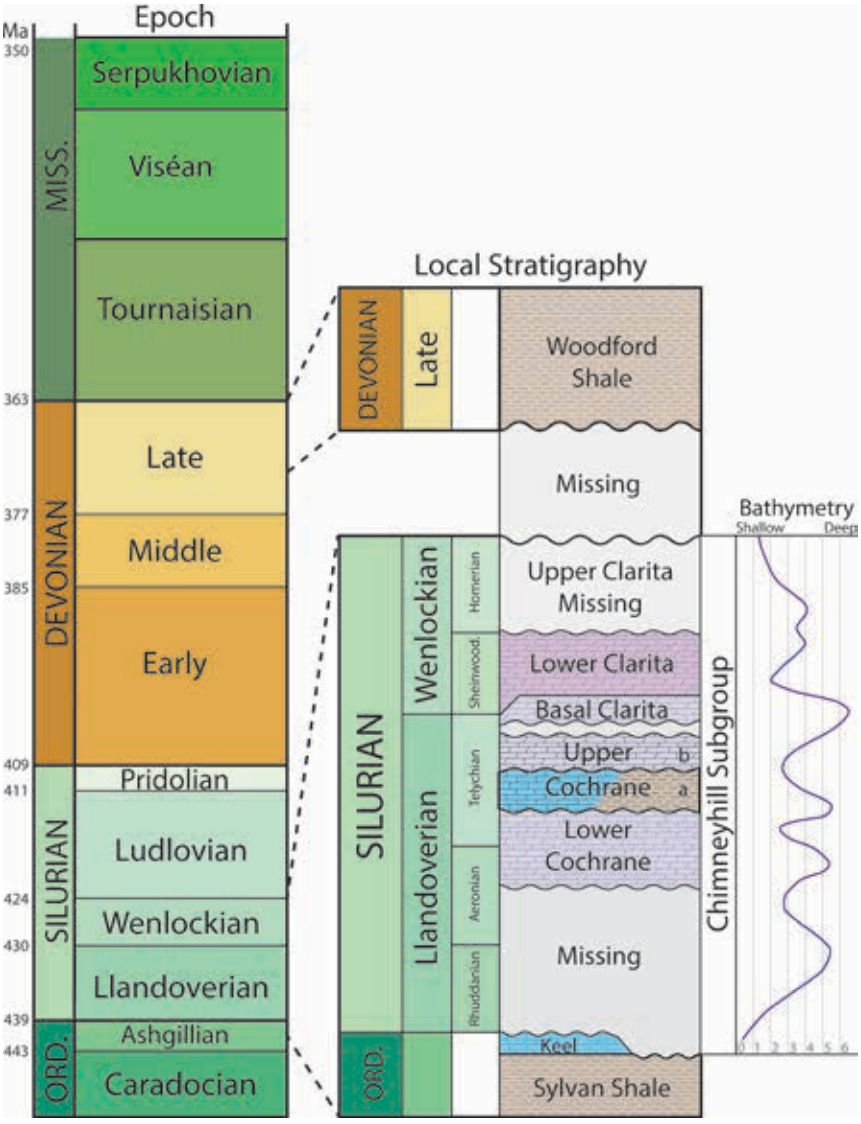

Figure 3. Stratigraphic column in the WCHF area. Only the Cochrane and the lower Clarita formations are present in the study area (after Derby, 2007).

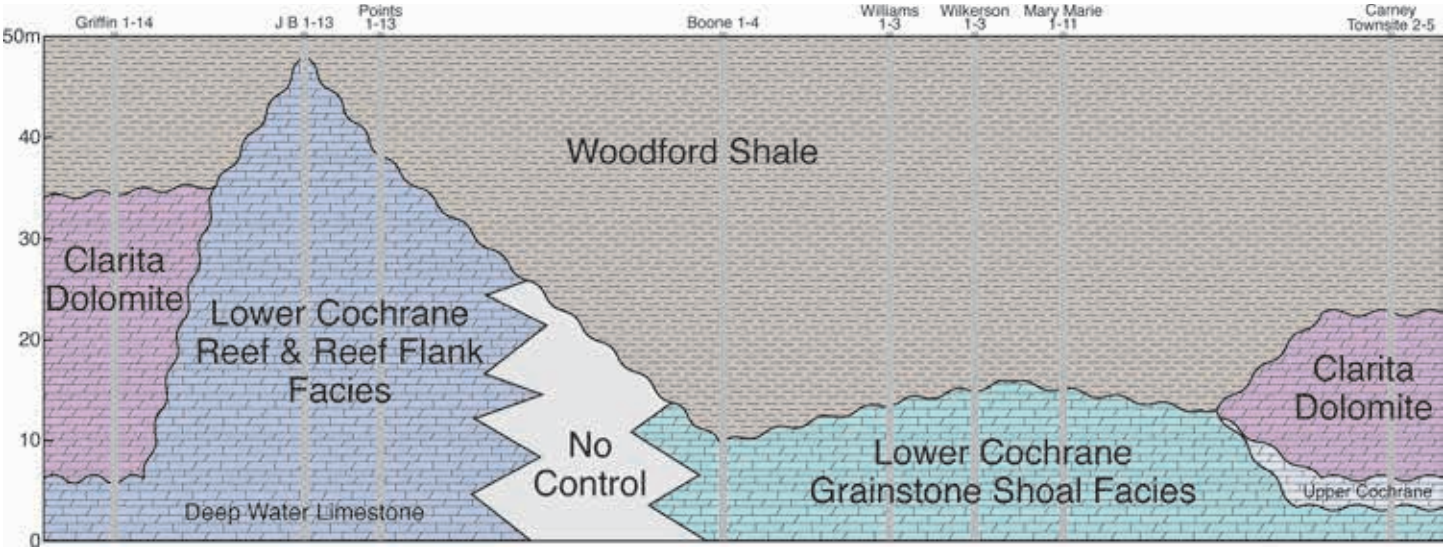

Figure 4. Schematic west to east cross section across the West Carney field area. The line of the section is shown on fig.1b. The lower Cochrane transitions from reef and reef flank facies in the west part of the field to a grainstone shoal facies in the central and eastern part of the field (after Derby et al., 2002b; Derby, 2007). Note that the Stevenson 1-14 and McBride South 1-10 wells (shown on fig. 1b) were not used to construct this section because a significant portion of the section was not cored in these wells.

the upper Cochrane B member (fig. 3). In the WCHF study area, the lower Cochrane member consists of brachiopod and crinoidal grainstones and packstones from the reef and reef flank and grainstone shoal megafacies (fig. 4) (Derby, 2007). The upper Cochrane member and most of the Clarita Formation are absent because of the relatively high paleotopography in the study area (paleo highs up to 30 m [98 ft]), except for outliers of the Clarita on the flanks of the WCHF (Braimoh, 2010) (fig. 4). This exposed paleotopographic high may have resulted from local structural uplift prior to deposition of the upper Clarita (Braimoh, 2010). The resulting paleo high prevented the deposition of more carbonates overlying the lower Cochrane member, resulting in the unconformable contact of the lower Cochrane with the overlying Misener Sandstone and Woodford Shale in the study area.

Derby (2007) described the lower Cochrane member as a reef-dominated carbonate shoal overlying deep-water carbonates that formed as an isolated platform in the early Silurian sea. Stratigraphic continuity of the reef carbonates is poor, lateral transitions are abrupt, and traceable subdivisions within the unit are rare. Subaerial weathering of the Hunton, during lowstands of the Silurian Sea, resulted in the development of karst-related porosity. Every well in the field shows evidence of multiple periods of karsting throughout the full thickness of the Hunton (Derby, 2007). Conventional intercrystal porosities are developed in the dolomitic facies as well. Dolomitization here resulted in enhanced porosity and permeability. However, the dolomitized sections are not continuous across the field and the processes that lead to dolomitization are unclear (Derby, 2007) and are addressed here.

METHODS

A total of 315 m (1,033.5 ft) of core from 19 wells (fig. 1b) was described in detail. The cores were provided by the Marjo Operating Co., Inc., Tulsa, Oklahoma. Detailed lithological descriptions of individual cores used in this study are available in Silva (2012), Smith (2012), and Ray (2018). Eight of these wells were cored in the lower Clarita Formation and eleven in the Cochrane Formation. Additional core descriptions are available in Derby (2007) and Braimoh (2010).

Wireline logs from 104 wells were correlated to generate isopach maps of the reservoir using IHS Petra (fig. 5). IHS Petra also was used to correlate gamma ray, photoelectric, and porosity logs. Correlation was based upon determination of the top of the Hunton carbonates, top of the Sylvan Shale, and dolomitic facies within the reservoir. The tops of the Hunton Group and Sylvan Shale were picked using gamma ray logs. Dolomite was distinguished from limestone using neutron porosity (φN) and density porosity (φD) logs (fig. 5).

Two hundred twenty polished standard thin sections were prepared from billets cut from cores. Sixteen additional oversized thin sections were provided by Marjo Operating Company. Limestone, partially dolomitized limestone, and dolomite lithologies were sampled. Both

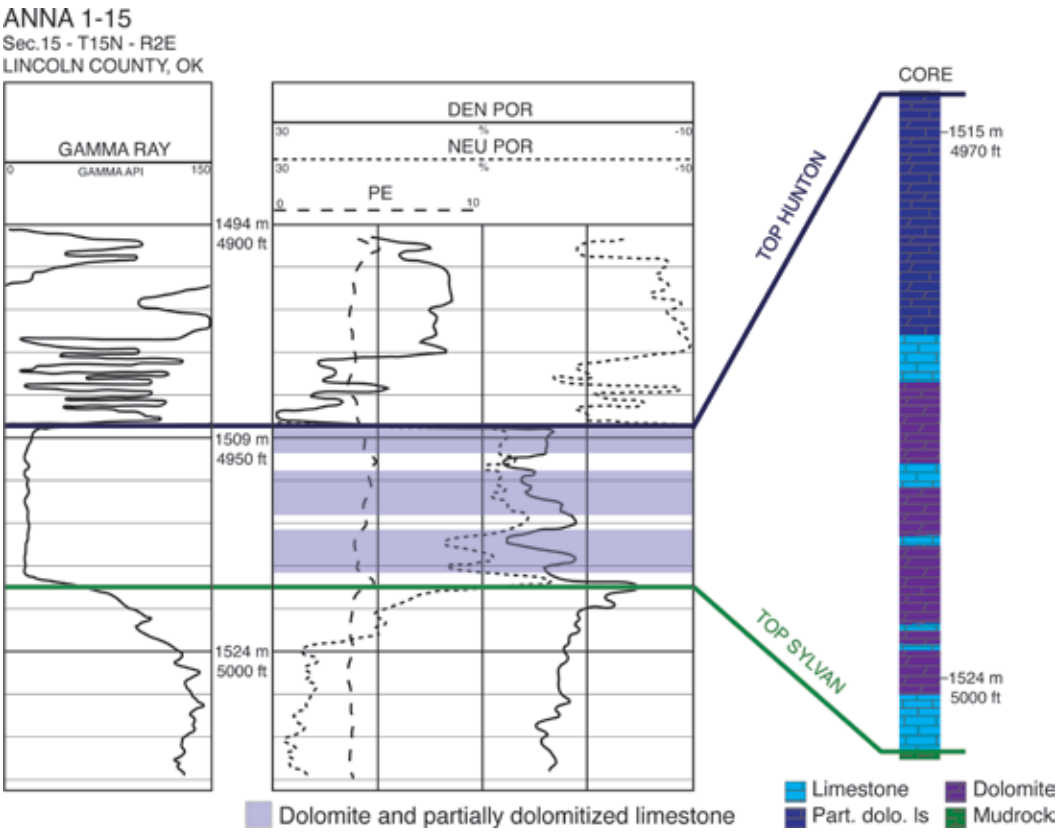

Figure 5. Type log for the WCHF, Anna 1-15 oil well and core (sec 15, T. 15 N., R. 2 E., Lincoln County, Oklahoma). The wireline log includes gamma ray (left) and neutron porosity (φN), density porosity (φD), and photoelectric effect (PE) (center). A lithological log, based on the core description, is shown on the right.

thin sections and core samples were stained with alizarin red-S and occasionally with potassium ferricyanide using the methods of Friedman (1959). Limestone fabrics were classified according to Dunham (1962), and diagenetic features, including pore types, were described using the classification system of Choquette and Pray (1970). Dolomite was described following Sibley and Gregg (1987). Description of grain and crystal size uses the terminology of Folk (1959). Total porosity was estimated from counts of 600 points per thin section. Cathodoluminescence (CL) petrography was conducted using a CITL CL 8200 MK5-1 Optical CL System mounted on an Olympus BX51 petrographic microscope. Photomicrographs using transmitted and CL light were obtained with a Q-Imaging Micropublisher 5.0 RTV cooled camera.

X-ray diffraction (XRD) analyses of selected powdered samples were made using a Philips Analytical PW 1830/00 diffractometer with Cu*K*α X-radiation at Oklahoma State University. Scanning electron microscopy (SEM) and energy-dispersive X-ray spectroscopy (EDS) of three dolomite samples were measured using a FEI Quanta 600 F field emission SEM at Oklahoma State University.

Fluid inclusion microthermometric analyses were conducted on sulfates (celestite) using a Linkam THMSG 600 heating and cooling stage mounted on an Olympus BX41 microscope equipped for UV epifluorescence. Standards and reproducibility of data for homogenization temperatures (T_h) and final ice melting temperatures (T_m) have errors of ±1.0°C and ±0.3°C, respectively. The equations of Bodner (1993) were used to calculate NaCl equivalencies (salinities) from T_m measurements. No corrections were made for pressure.

Prior to sampling for isotope geochemistry, limestone and dolomite samples were stained and examined petrographically to clearly distinguish calcite from dolomite and to identify compositional zones in calcite cements. The isotope composition of the carbonates was determined using the Krishnamurthy et al. (1997) method. Carbonate samples from the Cochrane Formation were measured using a Thermo-Finnigan Delta Plus gas-source isotope ratio mass spectrometer at Oklahoma State University. Clarita carbonate samples were measured using a Thermo-Finnigan Delta Plus gas-source isotope ratio mass spectrometer at the University of Missouri. Resulting $\delta^{13}C$ and $\delta^{18}O$ values are reported relative to VPDB with standard errors of less than ± 0.1%, based on replicate analyses of interlaboratory standards.

RESULTS

Subsurface Mapping of the Reservoir

The Hunton Group isopach map illustrates an overall heterogeneity in the reservoir thickness (fig. 6a). The

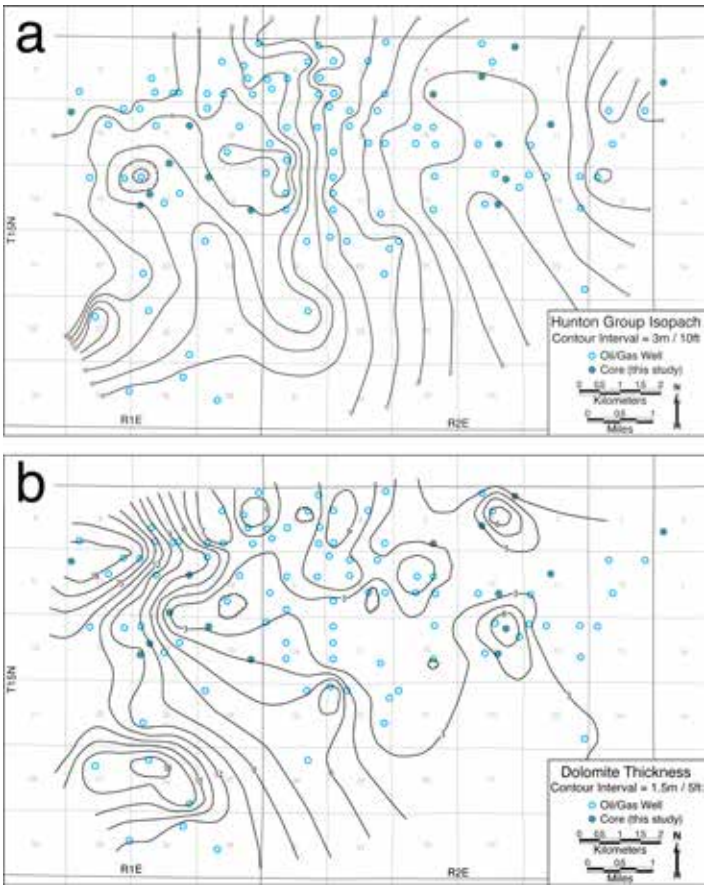

Figure 6. (a) Isopach map of the Hunton Group in the WCHF study area. (b) Cumulative thickness of dolomite in the study area calculated using wireline logs. The cumulative thickness of the dolomitic facies is greatest to the west where the carbonates section is thicker and the Clarita dolomite overlays the lower Cochrane.

Hunton is relatively thin in the eastern part of the study area, with an average thickness of 15.2 m (50 ft), and thickens westward to more than 40 m (130 ft). The dolomite facies cumulative thickness map (fig. 6B) generally mimics the Hunton Group isopach map. Dolomite thickens westward where the Hunton Group is the thickest and is thinner eastward where the Hunton Group is the thinnest. However, individual dolomitized strata are difficult to correlate from well to well.

Core Lithology

The lower Cochrane member comprises pink, yellow, tan, and white grainstones, dolomitic limestone, and crystalline dolomite (fig. 7). Sharp unconformable contacts were observed with the overlying Misener Sandstone Member of the Woodford Shale (fig. 7a) and with the underlying Sylvan Shale (fig. 7e). Skeletal components consist of brachiopods, crinoids, and occasional tabulate coral fragments. (See Derby [2007] for detailed paleontology). Packstones and boundstones containing pentamerid brachiopods (fig. 8) form the reef and reef flank megafacies (fig. 4). Brachiopod grains typically are larger than 2 mm and unreplaced by dolomite. They frequently are dissolved, leaving moldic porosity (fig. 7c). Crinoid and coral grains are much less common than brachiopods, are frequently larger than 2 mm, and are typically (but not entirely) unreplaced by dolomite.

The Clarita Formation consists of grayish yellow, pale grayish orange, very light brown, and light gray to black packstones and grainstones. Wackestones and mudstones are present but less common than packstones and grainstones (fig. 9). Crinoids are prevalent throughout the Clarita. The crinoids are frequently partially to completely dissolved, leaving moldic pores. Occasionally the cemented central canal of the crinoid is all that remains. In cases where crinoids are not dissolved, they are partially to completely replaced by dolomite. Other faunas observed in the Clarita include ostracodes, corals, gastropods, bryozoans, bivalves, trilobites, and, occasionally, nautiloids.

Dolomite is not distributed uniformly throughout the WCHF. With the exception of the Mary Marie 1-11 core, where dolomite was not observed, all cores described in the Cochrane Formation are slightly to extensively dolomitized (figs. 7 and 8). All of the Clarita Formation cores are partially to completely dolomitized (fig. 9). In core, the dolomite typically is fine to medium crystalline and frequently displays sucrosic texture (terminology of Choquette and Pray, 1970).

The most common pore types observed in core, in the limestone lithologies in the Cochrane Formation, are interparticle, intraparticle, vug, moldic, shelter, and fracture. The most common pore types in the dolomitic lithologies are intercrystal, moldic, solution-enlarged molds, vug, and shelter. The partially dolomitized limestone lithologies in the Clarita display interparticle, vug, and intraparticle pores. The Clarita dolomite lithology exhibits intercrystal porosity, well-developed moldic porosity, and solution-enlarged vugs largely due to the dissolution of crinoid grains.

Diagenetic features, such as stylolites and fractures, are present in both limestone and dolomite lithologies. Stylolites frequently are observed, and amplitudes range from less than 1 mm to 25 mm (figs. 7 and 9). Stylolites commonly bound the dolomitic lithologies (fig. 7b), indicating that dolomitization occurred prior to pressure-solution. Horizontal, vertical, and sub-vertical fractures cut the Hunton with no distinction between sedimentological

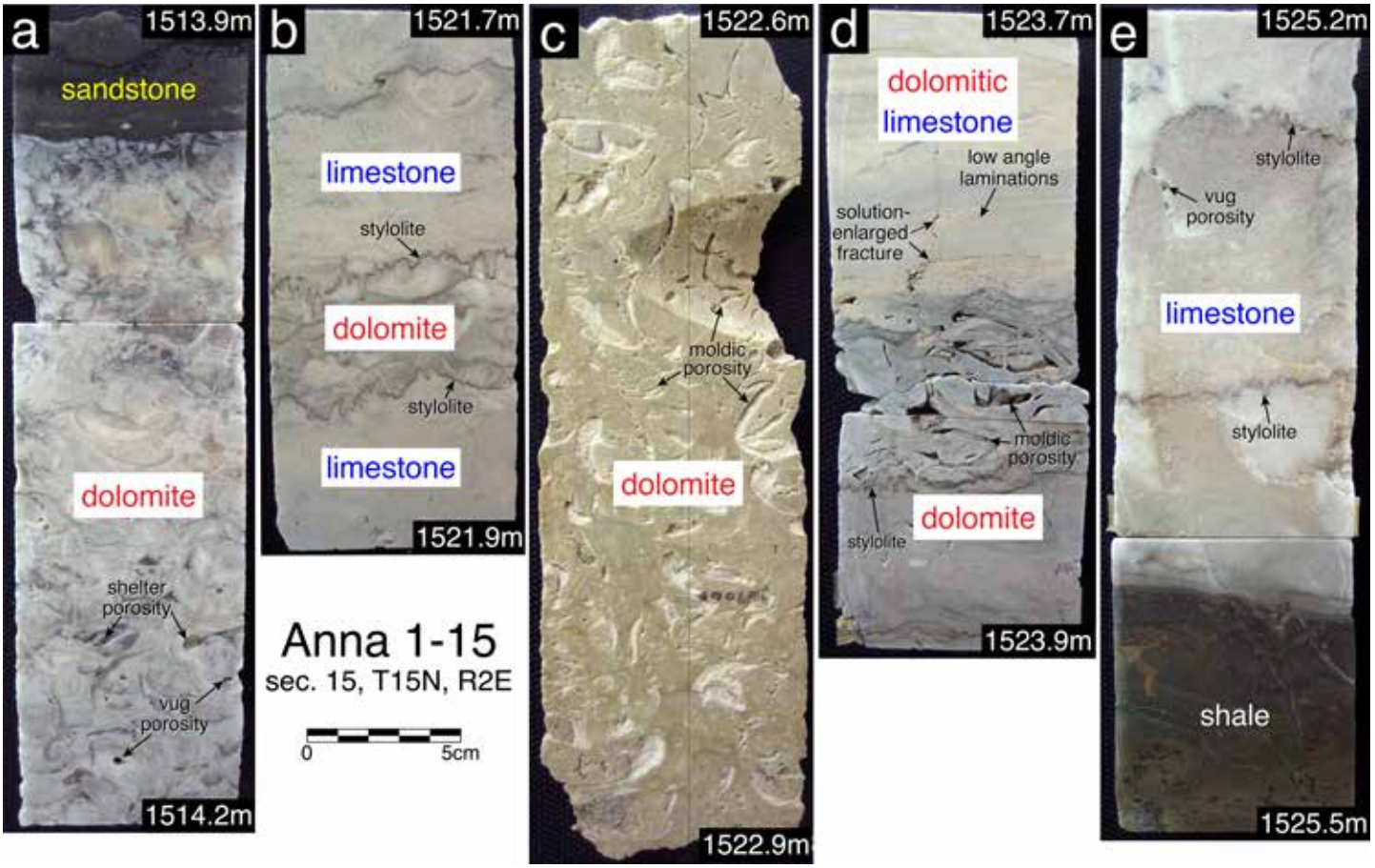

Figure 7. Representative core slab photographs from the Anna 1-15 well displaying dolomitized and partly dolomitized lithofacies in the grainstone shoal facies of the Cochrane Formation. Scale = 5 cm. (a) Misener Sandstone Member of the Woodford Shale (dark gray), with silicified brachiopod fragments, unconformably overlies a dolomitized brachiopod grainstone in the Cochrane Formation (white-light gray). (b) Dolomitized brachiopod grainstone (gray) bounded by stylolites. Limestones (white-light gray) both underlie and overlie the dolomite. (c) Dolomite replacing the matrix of a brachiopod packstone/wackestone. Undolomitized brachiopods have undergone partial leaching, generating moldic porosity. (d) Dolomite (gray) in contact with overlying slightly dolomitized limestone (white-light gray). Moldic porosity forms small megapores (5 to 20 mm) within the dolomite. A horizontal solution-enlarged fracture also is visible in the dolomite. Low-angle laminations are visible in the dolomitic limestone. (e) Undolomitized crystalline limestone with stylolites (white-light brown) unconformably overlying the Sylvan Shale (dark gray).

or diagenetic lithological features. Fractures are most commonly open or filled by siliciclastic sand, silt, and mud. Infrequently, fractures are filled by calcite cement indicating, in these cases, that fracturing occurred prior to calcite cementation. Two major types of breccias are observed in the Hunton: early sedimentary breccias (fig. 9c) that predate most diagenetic events and karst breccias that typically postdate calcite cementation (fig. 9b).

Karst features observed in core include breccias (figs. 9b–c); solution-enlarged fractures, frequently filled with siliciclastic clay and silt (figs. 7d and 9d); and large vugs (fig. 8). There is a large (3 m [10 ft]) cavern within the lower Cochrane observed in the Mark Houser 1-11 core from 1,542.6 to 1,545.9 m (5,061 to 5,072 ft), which has been completely filled with bioclasts and intraclasts as well as mud. This filling can be described as a partly dolomitized breccia supported by a fine to coarse cave fill matrix. No cave dripstones or flowstones were observed in the study area.

Thin Section Petrography

Limestone lithologies observed in thin section include coarse brachiopod-crinoid packstones and grainstones with intermixed wackestones. Skeletal grains throughout include brachiopods, tabulate corals, bryozoa, ostracodes, and trilobites (rare).

Dolomite observed in thin section displays planar-s and planar-e (sucrosic) textures and replaces precursor limestone (fig. 10a–d). Open-space-filling saddle dolomite cement was rarely observed and then only in the Clarita Formation, where saddle dolomite partially fills open spaces in the lower portion of the W. Carney Ext. SWDW 2

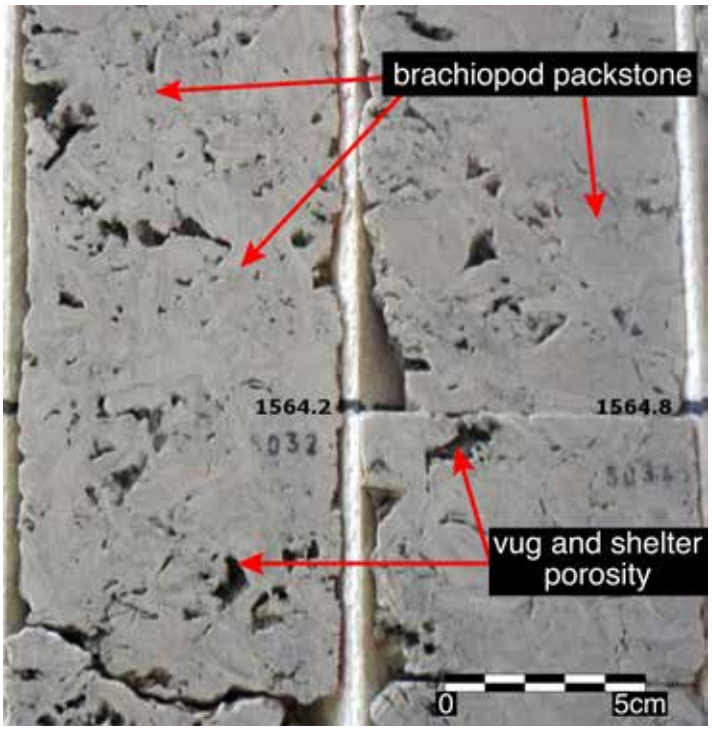

Figure 8. Representative core slab photographs from the Points 1-13 core from 1,563 to 1,564.8 m (5,128 to 5,134 ft): lower Cochrane limestone, pentamerid brachiopod packstone (reef facies) with well-developed shelter and vug porosity. Macropores display evidence of leaching. Core slabs are approximately 7.6 cm wide. Scale = 5 cm.

core (fig. 1b). Replacive dolomite crystal size distributions are typically unimodal and rarely polymodal with average crystal sizes from 0.04 mm to about 0.2 mm (fine to medium crystalline) and rarely up to 1.1 mm (very coarse crystalline). Dolomite crystals typically replace lime mudstone and, less typically, skeletal grains and are not observed to replace calcite cements (fig. 10). Frequently, however, brachiopods, corals, and crinoids, particularly in the Clarita Formation, are either unreplaced by dolomite or are preserved as fossil molds that may be partially to completely filled by calcite cement (fig. 10c–f). Partial dissolution (leaching) of dolomite crystals is observed, particularly adjacent to solution-enlarged vugs and fractures. Dolomite crystals frequently display evidence of partial replacement by calcite cement (dedolomitization), particularly in the Cochrane Formation (fig. 11a).

X-ray diffraction analysis of seven dolomite samples from the Carter Ranch 2-15 core (fig. 1b) display strong dolomite ordering reflections of (101), (015), and (021) (cf. Gregg et al., 2015) and an average stoichiometry of 52.8 ±1.5 mole % $CaCO_3$ (calculated using the method of Lumsden, 1979). Dolomite stoichiometry was confirmed by semi-quantitative FESEM-EDS analysis of three samples of dolomite that also indicate up to a few % Fe substitution in the dolomite crystal lattice.

Cathodoluminescence (CL) responses of dolomite in the Cochrane Formation typically display three distinct zones. From earliest to latest, these are CL Zone 1 (D1), an orange-red bright CL; CL Zone 2 (D2), dull CL; and CL Zone 3 (D3), thin-banded bright CL (fig. 11a). A fourth CL zone (D4) comprising a thin non-CL band occasionally was observed (Fig. 11a). The distribution of these CL zones varies among cores in the Cochrane Formation. The D1 zone is present in all cores and displays variation ranging from a mottled CL pattern to faint internal banding. The D2 and D3 zones do not exhibit variations in any of the cores where they were identified. In the Clarita Formation, up to five distinct CL zones were identified in planar-e dolomite crystals (fig. 11b). Planar-s dolomite textures in the Clarita typically lack distinct zonation. Rather, they exhibit either a moderate bright or mottled CL response (fig. 10d).

Calcite cements are observed in intergranular space, fossil molds, shelter porosity, vugs, and fractures in both limestone and dolomitic lithologies (fig. 10c–f). Compromise boundaries between cement crystals commonly display sharp edges. Mold and shelter pores typically exhibit a layer of radial prismatic cement growing into adjacent open space followed by blocky calcite cement. Intergranular and intragranular space frequently is filled by blocky calcite cement. Syntaxial overgrowths on crinoid grains are always followed by blocky calcite cement. Fracture fills are characterized by coarse to very coarse (0.5 mm to 3.0 mm) blocky calcite cement. Blocky calcite cements commonly exhibit twinning. Potassium ferricyanide staining was attempted, but none of the calcite cements observed have iron contents high enough to yield a positive stain.

Three distinct CL zones were observed in calcite cements throughout the study area (fig. 10f). Their distributions, however, vary from core to core and with stratigraphic position. The three zones, from earliest to latest cement, are the following: CL Zone 1 (Z1) composed of a non-CL cement. CL Z1 occurs as syntaxial overgrowths on crinoid grains as well as the first generation of open-space-filling cement where crinoids are not present. CL Zone 2 (Z2) typically follows Z1 and includes a thin band of bright CL followed by a thin non-CL cement. CL Zone 3 (Z3) comprises numerous sub-zones consisting of alternating bright and dull CL bands. Z3 typically is the last generation of cement and occludes much of the primary pore space in the reservoir. Calcite cement partially replaces dolomite crystals (i.e., dedolomite) throughout the WCHF.

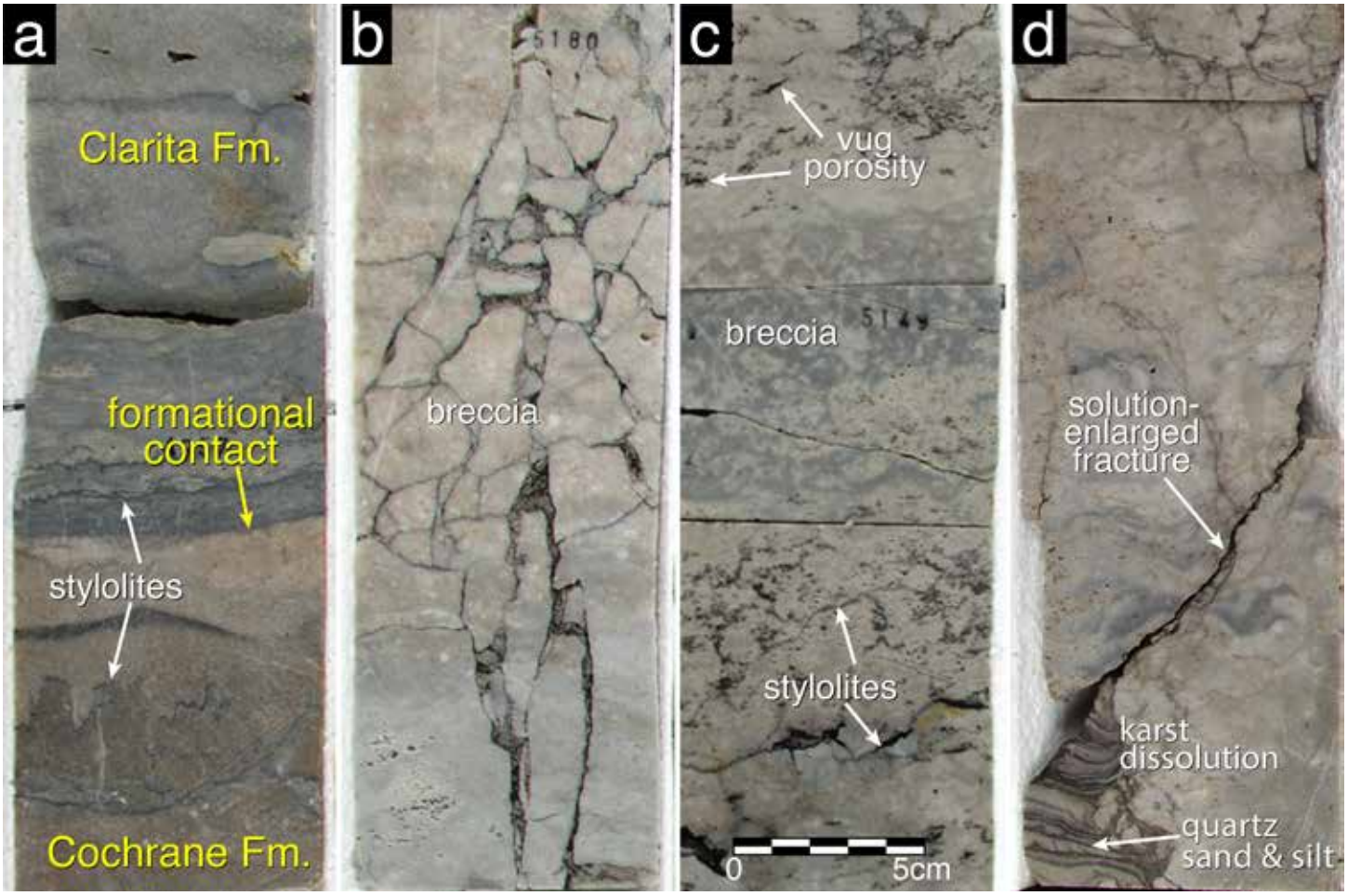

Figure 9. Representative core slab photographs from Clarita Formation cores comprising dolomitized grainstones, packstones, and mudstones. Scale = 5 cm. (a) Contact between the Clarita and Cochrane Formations in the Carney Townsite 2-5 core. Note high amplitude stylolites in uppermost Cochrane and lower amplitude stylolites in the lowermost Clarita. (b) Karst breccia porosity in the W. Carney Ext. SWDW 2 core. (c) Early sedimentary breccia and stylolites in the Stevenson 1-14 core. (d) Sub-vertical solution-enlarged fracture and karst dissolution cavity filled with laminated clastic quartz sand and silt (lower left) in the Griffin 1-14 core.

Silica cement in the form of authigenic quartz is relatively rare in the WCHF study area and paragenetically follows Z3 calcite. Silica cement was only observed near the Hunton Group–Sylvan Shale contact. Large celestite crystals (0.5 to 21 mm) were observed filling vug porosity in both the Carney Townsite 2-5 and Geneva 2-32 cores in the Clarita Formation on the east side of the WCHF (fig. 1). In both instances where celestite cements were observed, the celestite paragenetically followed Z3 calcite cement and occurred proximal to the Sylvan Shale contact.

Limestone pore types observed in thin section include shelter, vuggy, intergranular, intragranular, fracture, and dissolution porosity. Porosity values in limestone, determined by point count, range from less than 1 to 8%, with the majority of limestone thin sections in the range of 1% porosity. Porosity in limestone lithologies frequently is occluded by blocky calcite cement and syntaxial overgrowths of calcite cement on crinoid grains. Higher porosity values were observed in areas where dissolution occurs, in facies containing an abundance of brachiopods, and in partly dolomitized and completely dolomitized intervals where pores are better connected. The most frequent pore types in the dolomite lithologies, as observed in thin section, are intercrystal, vug, moldic, fracture, shelter, intraparticle, and interparticle. Vugs and molds frequently range in size up to 0.5 cm and fractures from less than 0.1 to 1.5 mm wide. Pore space in dolomite frequently is filled by calcite cement (fig. 10c–d). Large open spaces frequently are filled with karst sediment, including clay, silt, and fine quartz sand grains, likely derived from the overlying sediments (fig. 10e–f). Porosity in dolomite, calculated from thin section point counts, ranges from 0 to 24%. The highest porosities occur in association with solution-enlarged molds, vugs, and fractures.

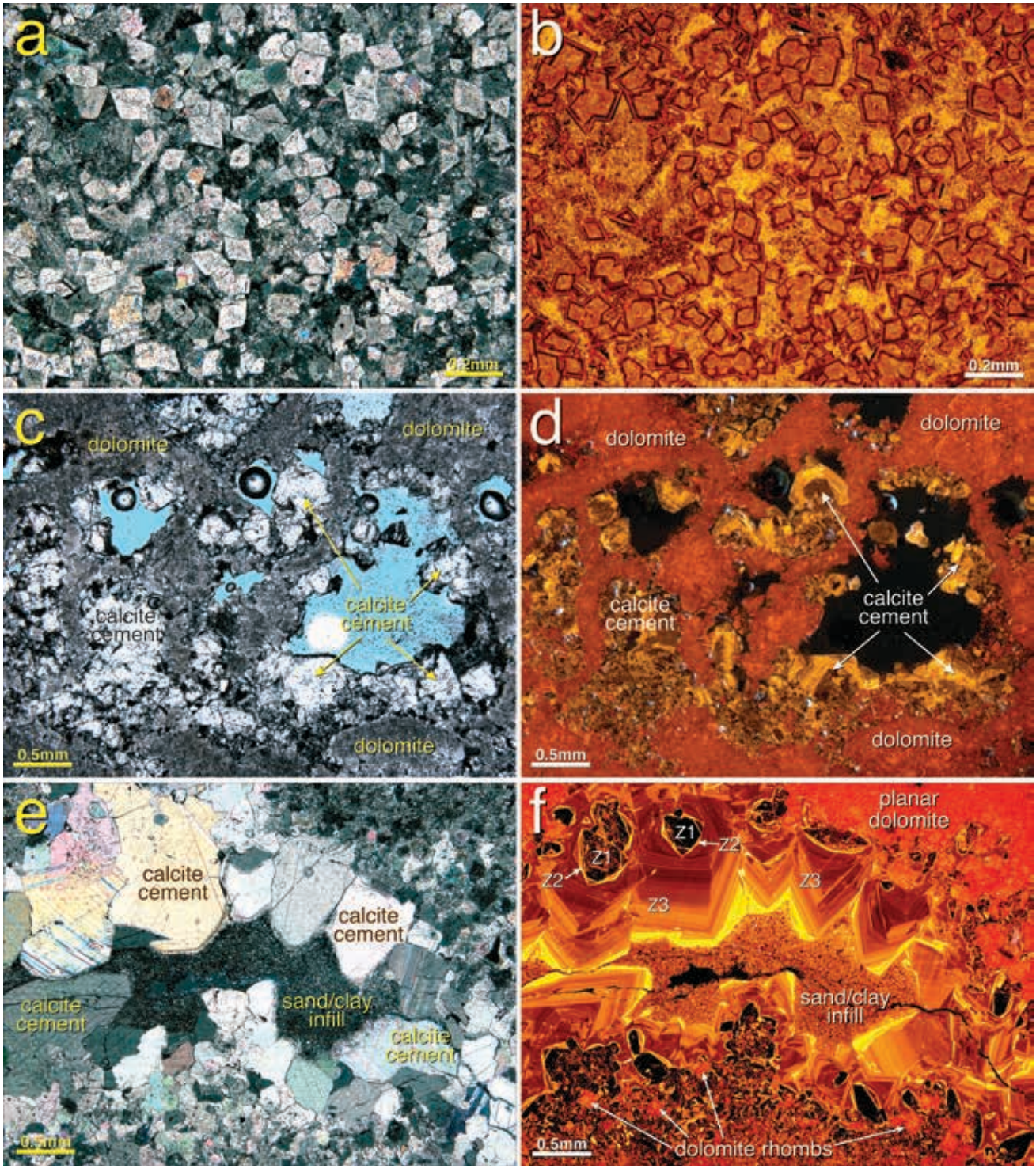

Figure 10. Photomicrographs of replacement dolomite and later diagenetic alteration: (a) Planar dolomite replacing a skeletal wackestone in the Points 1-13 core at 1,556.5 m (5,107 ft). Scale = 0.2 mm. (b) CL of the same field of view as (a) showing partial replacement of limestone (yellow to orange CL) by dolomite displaying dark red to reddish orange compositional zoning of the dolomite crystals. Scale = 0.2 mm. (c) Dolomitized skeletal grainstone/packstone in the Clarita Formation with vuggy (moldic?) pores partially occluded by open-space-filling blocky calcite cement. Sample is from the Bailey 2-6 core. Scale = 0.5 mm. (d) CL of the same field as (c). Red areas are replaced by planar-s dolomite. Note yellow-orange zoned calcite cement filling open spaces. Scale = 0.5 mm. (e) and (f) Large vug in the Mark Houser 1-11 core. Several diagenetic features are observed: 1. Partial replacement of host limestone by dolomite, which displays the three-zone CL microstratigraphy typical of the Cochrane Formation. 2. Dissolution of the host limestone/dolomite, forming the vug. 3. Open-space-filling calcite cement displaying a distinctive three-zone CL compositional zoning (Z1, Z2, and Z3). 4. Siliciclastic infill of sand and clay, which likely is sourced from the overlying Misener Sandstone and Woodford Shale (fig. 7a). Scale = 0.5 mm

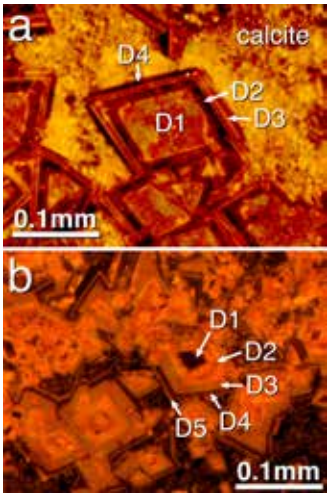

Figure 11. CL photomicrographs showing zonation. (a) Dolomite CL zones in the Cochrane Formation from the Points 1-13 core at 1,556.5 m (5,107 ft). Zone D1 is the earliest and displays orange-red bright CL. D2 displays reddish-gray dull CL. D3 is the latest and displays thin bands of reddish-orange bright CL. D4 is visible on several crystals and consists of a non-CL outer band. Scale = 0.1 mm. (b) Dolomite CL zones in the Clarita Formation from the Mercer 1-28 core (1,385 m [4,544 ft]). Zone D1 is non-CL, D2 is bright multi-banded CL, D3 is moderately bright multi-banded CL, D4 is dull to non-CL, and D5 is a non-CL band followed by a bright outer band. Scale = 0.1 mm.

Fluid Inclusion Microthermometry

Two-phase (liquid-vapor) fluid inclusions were not observed in calcite or dolomite cements. Two-phase (liquid-vapor) primary and secondary aqueous fluid inclusions, along with several possible three-phase (liquid-solid-vapor) inclusions, were observed in open-space-filling celestite crystals. Many of the inclusions display negative crystal morphology. Necking down of inclusions was occasionally observed. A total of 83 inclusions (25 primary and 58 secondary) yielded both T_h and T_m values and were grouped into 14 assemblages (table 1). The fluid inclusions that were measured ranged in long dimension from 20 to 200 μm. Smaller inclusions were observed, but they were not measured due to poor optical resolution. Measured T_h values of primary inclusions ranged from 186 to 272°C, and calculated salinities based on T_m values ranged from 16.1 to 21.5 equivalent weight % NaCl. Secondary fluid inclusion T_h values ranged from 148 to 286°C with salinities ranging from 18.5 to 22.4 equivalent weight % NaCl. Petroleum inclusions were identified among the secondary inclusions using UV epifluorescence. Two hues of fluorescence were observed — pale yellow and pale blue — indicating a range of medium to light oils (~25° and ~45° API gravity respectively) (Goldstein and Reynolds, 1994).

Isotope Geochemistry

Stable carbon and oxygen analyses for limestone (calcite) and dolomite lithologies in the WCHF are given in tables 2 and 3, respectively. These values are plotted on fig. 12. Values for brachiopods, determined to be largely unaltered by diagenesis, and crinoids are all from the Cochrane Formation and fall close to the expected values for calcite precipitated in equilibrium with Llandoverian seawater (Azmy et al., 1998). Both early (Z1) and late (Z2 and Z3) calcite cements were sampled in the Cochrane Formation. Calcite cements in the Clarita Formation were sampled in bulk but consist mostly of Z2 and Z3 cement. Due to the frequency of calcite inclusions (dedolomite), dolomite values may be affected by some contamination with later calcite cement.

Table 1. Fluid inclusion microthermometry of celestite crystals filling solution-enhanced vugs in the Cochrane Formation.

Geneva 2-32 1491.7m

Chip-Assemblage	Th (°C)	Tm (°C)	Eq. Wt.% NaCl	FI Type
1-1	185.6	-17.7	20.7	Primary
	233.5	-17.1	20.3	Primary
	233.5	-17.6	20.7	Primary
1-2	194.9	-13.9	17.7	Secondary
	205.1	-16.8	20.1	Secondary
	194.9	-14.4	18.1	Secondary
1-3	191.5	-15.9	19.4	Secondary
	155.0	-16.6	19.9	Secondary
	155.0	-16.7	20.0	Secondary
	221.3	-14.6	18.3	Secondary
	248.0	-15.6	19.1	Secondary
	233.1	-15.8	19.3	Secondary
	148.4	-14.8	18.5	Secondary
	171.0	-14.5	18.2	Secondary

Geneva 2-32 1491.7m

Chip-Assemblage	Th (°C)	Tm (°C)	Eq. Wt.% NaCl	FI Type
1-4	218.2	-16.6	22.4	Secondary
	199.2	-16.9	20.1	Secondary
	221.6	-16.9	20.1	Secondary
	197.6	-16.7	20.0	Secondary
	200.0	-16.6	19.9	Secondary
	204.5	-17.1	20.3	Secondary
	206.0	-17.1	20.3	Secondary
	201.7	-16.5	19.8	Secondary
	202.9	-16.4	19.8	Secondary
	203.4	-16.5	19.8	Secondary
	220.0	-16.8	20.1	Secondary
	197.5	-17.4	20.5	Secondary
	205.4	-17.1	20.3	Secondary
	192.6	-17.0	20.2	Secondary
	206.5	-16.4	19.8	Secondary
1-5	210.0	-16.1	19.5	Secondary
	219.5	-15.7	19.2	Secondary
	211.8	-16.5	19.8	Secondary
	210.3	-16.9	20.1	Secondary
	182.9	-17.3	20.4	Secondary
	200.3	-16.7	20.0	Secondary
	230.0	-16.4	19.8	Secondary
	219.5	-16.3	19.7	Secondary
	221.0	-15.7	19.2	Secondary
	201.3	-16.6	19.9	Secondary
	222.2	-16.8	20.1	Secondary
	207.0	-16.7	20.0	Secondary
2-1	215.0	-16.2	19.6	Primary
	203.0	-16.8	20.1	Primary
2-2	260.0	-17.9	20.9	Secondary
	237.1	-18.4	21.3	Secondary
	226.2	-18.1	21.0	Secondary
	248.6	-17.9	20.9	Secondary
	263.9	-18.7	21.5	Secondary
	217.7	-18.2	21.1	Secondary
	258.0	-18.5	21.3	Secondary
3-1	206.7	-18.7	21.5	Primary
	262.3	-17.9	20.9	Primary
	240.9	-17.6	20.7	Primary
	242.8	-16.1	19.5	Primary

Carney Townsite 2-5 1501.4m

Chip-Assemblage	Th (°C)	Tm (°C)	Eq. Wt.% NaCl	FI Type
1-1	131.2	-14.3	18.0	Secondary
	170.6	-15.2	18.8	Secondary
	162.0	-14.7	18.4	Secondary
1-2	214.3	-12.1	16.1	Primary
	225.0	-13.4	17.3	Primary
	229.6	-12.3	16.2	Primary
	271.9	-17.0	20.2	Primary
	262.7	-12.8	16.7	Primary
	262.5	-13.0	16.9	Primary

Carney Townsite 2-5 1501.4m				
Chip-Assemblage	**Th (°C)**	**Tm (°C)**	**Eq. Wt.% NaCl**	**FI Type**
1-3	256.0	-16.4	19.8	Secondary
	248.7	-16.6	19.9	Secondary
	247.0	-16.2	19.6	Secondary
1-4	256.2	-16.8	20.1	Primary
	258.4	-16.7	20.0	Primary
	241.7	-16.5	19.8	Primary
2-1	261.6	-19.1	21.8	Secondary
	211.6	-16.6	19.9	Secondary
	154.4	-15	18.6	Secondary
	172.0	-15.4	19.0	Secondary
	173.0	-18	21.0	Secondary
	175.0	-16	19.4	Secondary
	176.8	-17.4	20.5	Secondary
2-2	213.0	-17.3	20.4	Primary
	275.6	-18.1	21.0	Primary
	285.7	-18.3	21.2	Primary
	212.7	-18.1	21.0	Primary
	242.6	-17.3	20.4	Primary
	211.1	-16.6	19.9	Primary
	225.2	-19.6	22.1	Primary

Table 2. Stable carbon and oxygen isotope data for calcites in the Cochrane and Clarita Formations.

Cochrane Formation				
Core	**Depth (m)**	**Lithology**	**$\delta^{18}O$ ‰$_{VPDB}$**	**$\delta^{13}C$ ‰$_{VPDB}$**
Points 1-13	1,521.8	Brachiopod	-3.95	0.27
Points 1-13	1,524.8	Brachiopod	-3.56	0.89
Points 1-13	1,528.2	Brachiopod	-3.95	0.94
Points 1-13	1,530.9	Brachiopod	-3.94	1.21
Points 1-13	1,534.0	Brachiopod	-4.07	1.86
Points 1-13	1,536.4	Brachiopod	-4.26	0.75
Points 1-13	1,540.1	Brachiopod	-3.89	1.22
Points 1-13	1,543.1	Brachiopod	-4.36	1.58
Points 1-13	1,550.1	Brachiopod	-4.45	-0.79
Points 1-13	1,551.1	Brachiopod	-5.21	0.29
JB 1-13	1,515.4	Crinoid	-4.37	1.39
JB 1-13	1,518.4	Crinoid	-3.91	1.64
JB 1-13	1,518.4	Crinoid	-4.41	1.37
JB 1-13	1,517.8	Crinoid	-4.66	0.97
JB 1-13	1,521.2	Crinoid	-3.11	1.66
JB 1-13	1,521.5	Crinoid	-3.68	-4.68
JB 1-13	1,527.9	Crinoid	-4.01	1.69
JB 1-13	1,539.2	Crinoid	-3.70	1.60
Points 1-13	1,541.3	Crinoid	-2.80	1.28
Points 1-13	1,554.7	Crinoid	-4.39	3.48
JB 1-13	1,538.3	Calcite Cement (Z1 & 2)	-2.75	2.00
JB 1-13	1,540.4	Calcite Cement (Z1 & 2)	-5.05	-1.20
JB 1-13	1,541.3	Calcite Cement (Z1 & 2)	-2.80	1.29
Mark Houser 1-11	1,537.6	Calcite Cement (Z1 & 2)	-4.71	0.29
Mark Houser 1-11	1,546.5	Calcite Cement (Z1 & 2)	-4.52	1.71

Cochrane Formation

Core	Depth (m)	Lithology	$\delta^{18}O$ ‰$_{VPDB}$	$\delta^{13}C$ ‰$_{VPDB}$
Mark Houser 1-11	1,546.8	Calcite Cement (Z1 & 2)	-4.38	1.75
Mark Houser 1-11	1,546.8	Calcite Cement (Z1 & 2)	-4.00	1.62
Mark Houser 1-11	1,546.8	Calcite Cement (Z1 & 2)	-4.16	1.60
Mark Houser 1-11	1,546.8	Calcite Cement (Z1 & 2)	-7.83	-0.48
Points 1-13	1,528.2	Calcite Cement (Z1 & 2)	-5.43	-4.68
Points 1-13	1,534.0	Calcite Cement (Z1 & 2)	-5.86	-2.69
Points 1-13	1,555.0	Calcite Cement (Z1 & 2)	-6.16	-1.19
Cal 1-11	1,559.0	Calcite Cement (Z3)	-2.38	2.10
Cal 1-11	1,559.0	Calcite Cement (Z3)	-2.64	2.72
Cal 1-11	1,558.4	Calcite Cement (Z3)	-7.27	-0.20
Cal 1-11	1,558.4	Calcite Cement (Z3)	-3.02	1.38
Cal 1-11	1,534.6	Calcite Cement (Z3)	-5.30	-2.33
JB 1-13	1,538.3	Calcite Cement (Z3)	-7.25	-2.19
JB 1-13	1,540.4	Calcite Cement (Z3)	-3.54	1.98
JB 1-13	1,541.3	Calcite Cement (Z3)	-4.68	-0.65
Points 1-13	1,555.0	Calcite Cement (Z3)	-6.12	-1.20
Mark Houser 1-11	1,543.4	Calcite Cement (Z3)	-7.87	-0.50
Mark Houser 1-11	1,546.5	Calcite Cement (Z3)	-7.22	-1.75
Mark Houser 1-11	1,546.8	Calcite Cement (Z3)	-6.56	-1.28
Mark Houser 1-11	1,546.8	Calcite Cement (Z3)	-6.23	-1.34

Clarita Formation

Core	Depth (m)	Lithology	$\delta^{18}O$ ‰$_{VPDB}$	$\delta^{13}C$ ‰$_{VPDB}$
Bailey 2-6	1,489.5	Calcite Cement (Z1, 2 & 3)	-4.61	1.05
Chandler 1-5	1,469.1	Calcite Cement (Z1, 2 & 3)	-5.95	-0.21
Geneva 2-32	1,491.9	Calcite Cement (Z1, 2 & 3)	-3.53	2.88
Griffin 1-14	1,556.5	Calcite Cement (Z1, 2 & 3)	-9.59	-0.15
Griffin 1-14	1,561.1	Calcite Cement (Z1, 2 & 3)	-6.8	0.41
Mercer 1-28	1,381.6	Calcite Cement (Z1, 2 & 3)	-3.96	3.59
Stevenson 1-14	1,569.6	Calcite Cement (Z1, 2 & 3)	-3.92	1.69
West Carney Ext 2	1,573.0	Calcite Cement (Z1, 2 & 3)	-6.76	-0.64
West Carney Ext 2	1,573.0	Calcite Cement (Z1, 2 & 3)	-5.58	1.82
West Carney Ext 2	1,585.5	Calcite Cement (Z1, 2 & 3)	-6.46	-1.17

Table 3. Stable carbon and oxygen isotope data for dolomites in the Cochrane and Clarita Formations.

Cochrane Formation				
Core	**Depth (m)**	**Mineralogy (texture)**	**$\delta^{18}O$ ‰$_{VPDB}$**	**$\delta^{13}C$ ‰$_{VPDB}$**
Anna 1-15	1,521.9	Dolomite (planar replacive)	-3.90	0.27
	1,522.2	Dolomite (planar replacive)	-3.30	0.09
	1,523.8	Dolomite (planar replacive)	-3.47	0.04
	1,524.4	Dolomite (planar replacive)	-4.94	-0.36
Boone 1-4	1,540.1	Dolomite (planar replacive)	-4.95	0.51
	1,543.4	Dolomite (planar replacive)	-4.91	0.46
	1,544.0	Dolomite (planar replacive)	-4.67	-0.88
	1,544.2	Dolomite (planar replacive)	-2.80	-0.01
Cal 1-11	1,559.2	Dolomite (planar replacive)	-3.72	1.07
Carter Ranch 2-15	1,527.0	Dolomite (planar replacive)	-4.66	0.91
	1,528.8	Dolomite (planar replacive)	-3.56	0.56
	1,530.3	Dolomite (planar replacive)	-5.40	0.25
	1,532.2	Dolomite (planar replacive)	-3.51	0.13
	1,533.6	Dolomite (planar replacive)	-3.62	0.16
	1,533.8	Dolomite (planar replacive)	-3.62	1.60
JB 1-13	1,524.2	Dolomite (planar replacive)	-3.02	-0.69
	1,530.9	Dolomite (planar replacive)	-3.72	1.16
Mark Houser 1-11	1,545.5	Dolomite (planar replacive)	-4.51	1.14
	1,546.0	Dolomite (planar replacive)	-3.72	1.22
McBride South 1-10	1,513.3	Dolomite (planar replacive)	-6.53	-2.03
	1,514.2	Dolomite (planar replacive)	-3.76	-0.85
	1,515.0	Dolomite (planar replacive)	-3.53	0.72
	1,515.2	Dolomite (planar replacive)	-3.92	0.45
Points 1-13	1,556.5	Dolomite (planar replacive)	-1.43	1.30
Wilkerson 1-3	1,523.4	Dolomite (planar replacive)	-3.72	-0.92
	1,523.8	Dolomite (planar replacive)	-5.06	-0.63
Williams 1-3	1,517.6	Dolomite (planar replacive)	-4.47	-1.59
	1,518.8	Dolomite (planar replacive)	-4.04	-0.71
Clarita Formation				
Core	**Depth (m)**	**Mineralogy (texture)**	**$\delta^{18}O$ ‰$_{VPDB}$**	**$\delta^{13}C$ ‰$_{VPDB}$**
Bailey 2-6	1,489.3	Dolomite (planar replacive)	-2.34	1.74
	1,489.3	Dolomite (planar replacive)	-4.92	1.89
Chandler 1-5	1,466.4	Dolomite (planar replacive)	-5.39	1.65
	1,473.4	Dolomite (planar replacive)	-3.43	2.34
Carney Townsite 2-5	1,510.6	Dolomite (planar replacive)	-2.83	3.16
Geneva 2-32	1,508.5	Dolomite (planar replacive)	-5.58	2.49
Griffin 1-14	1,551.1	Dolomite (planar replacive)	-5.55	1.58
	1,551.1	Dolomite (planar replacive)	-5.83	1.08
Mercer 1-28	1,379.8	Dolomite (planar replacive)	-4.72	-7.19
	1,384.2	Dolomite (planar replacive)	-4.11	1.65
	1,385.3	Dolomite (planar replacive)	-3.81	1.61
Stevenson 1-14	1,573.7	Dolomite (planar replacive)	-6.23	3.22
West Carney Ext 2	1,572.8	Dolomite (planar replacive)	-5.08	1.18
	1,592.3	Dolomite (planar replacive)	-4.45	2.68

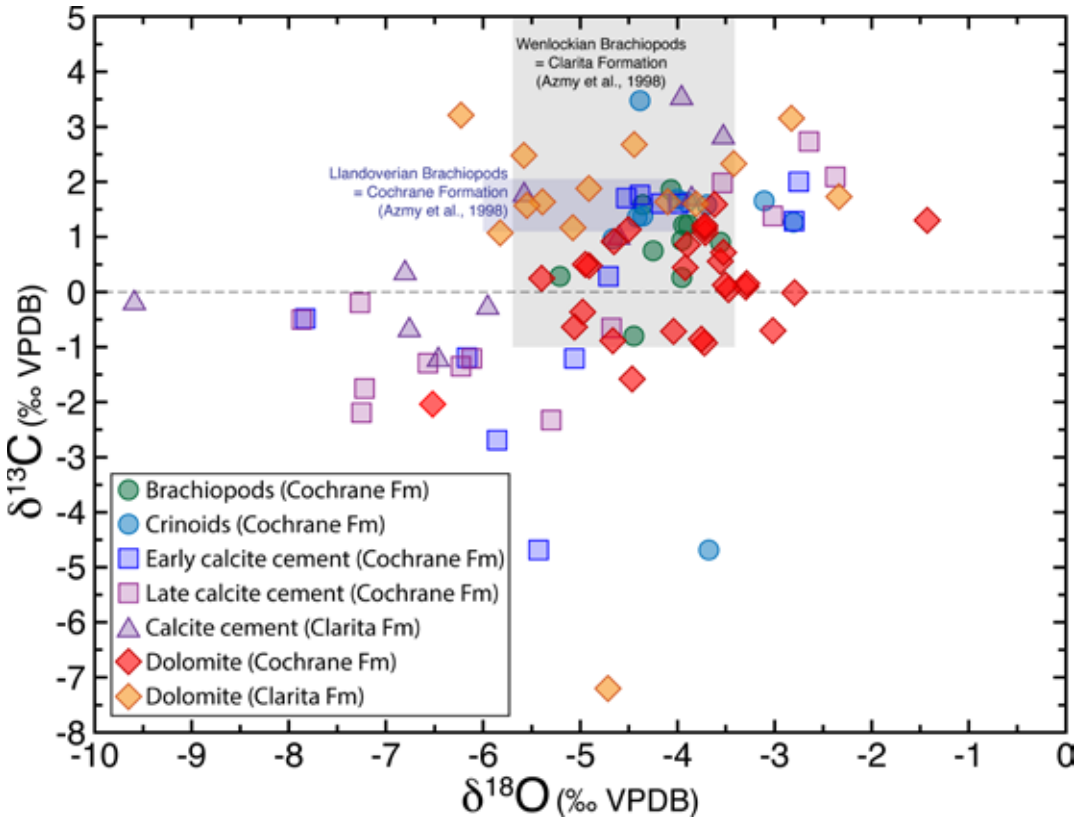

Figure 12. Stable carbon and oxygen isotope values for the WCHF carbonates. Fields are shown for Llandoverian and Wenlockian age brachiopods (assumed to represent low-magnesium calcite in equilibrium with seawater).

DISCUSSION

Early Limestones Diagenesis

Figure 13 shows a hypothesized sequence of diagenetic events related to sea-level change in the WCHF study area. Early diagenesis in the study area likely was affected by introduction of meteoric water during sea-level lowstands (figs. 3, 13b and e) and consisted mainly of neomorphic recrystallization of original aragonite and high Mg calcite skeletal grains to low Mg calcite (cf. Bathurst, 1975). This likely was accompanied by initial leaching of skeletal and other grains forming molds and dissolution of early fractures. Meteoric water diagenesis continued with each successive sea-level lowstand (fig. 13). The development of prominent karst features in the study area also occurred during multiple sea-level lowstands, when the WCHF area stood as a topographic high and was exposed to subaerial weathering (Derby, 2007). The rather pock-marked and irregular appearance of the Hunton Group isopach map (fig. 6a) is not an accident but is precisely what would be expected of a highly karsted limestone body. Larger-scale isopach and paleotopographical maps of the Hunton Group in the study area, with similar results, were constructed by Braimoh (2010). Karst features such as breccias, interconnected vugs, and solution-enhanced fractures occur throughout the Hunton (Derby et al., 2002b; Derby, 2007). No meniscus cements or microstalactitic cements are observed in any of the cores examined in this study to indicate meteoric vadose cementation.

Dolomite and Dolomitization

Timing of dolomitization in both the Cochrane and Clarita Formations is constrained by sedimentation of the host limestone during the Silurian and timing of calcite cementation (see discussion below) that postdates dolomitization. Although dolomite occasionally replaces calcite skeletal grains, it is never observed replacing open-space-filling calcite cements. Timing of much of the karst dissolution in the Cochrane and Clarita Formations also appears to postdate dolomitization as evidenced by dissolution of dolomite crystals, particularly adjacent to solution-enlarged open spaces. The CL characteristics of calcite that partially replaces dolomite (dedolomite) is similar to the CL Z2 and Z3 calcite cements, suggesting that the timing of dedolomitization corresponds to calcite cementation.

Dolomite in the WCHF displays planar-e and -s textures and primarily replaces the lime mud component of limestones and, less frequently, skeletal grains. Dolomite crystals typically range in size from fine to medium (0.04 to 0.2 mm) and rarely up to very coarse crystalline (greater than 1 mm). These fine crystals are typical of dolomites

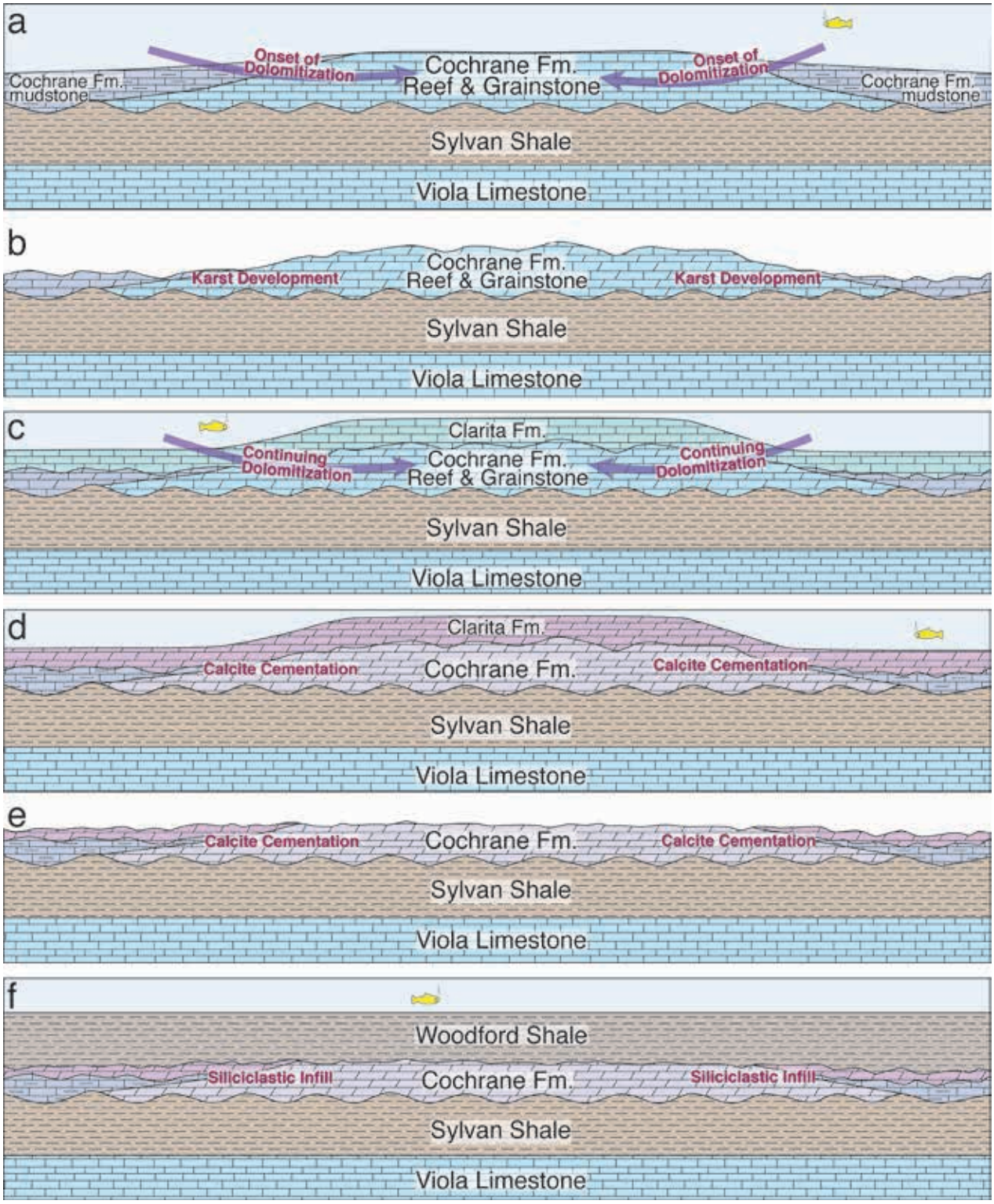

Figure 13. Hypothesized sequence of events in the WCHF study area: (a) Deposition and initial diagenesis of the Cochrane Formation, including probable initial onset of dolomitization by convective circulation of normal seawater. (b) Sea-level fall and development of an unconformity at the top of the Cochrane Formation and likely onset of karst development in the Cochrane Formation. (c) Rise in sea level with deposition and early diagenesis of the Clarita Formation and resumption of dolomitization of both the Cochrane and Clarita by convective circulation of normal seawater. (d) Open-space calcite cementation likely initiated after dolomitization. (e) Sea-level fall resulting in continuing calcite cementation, likely by mixed seawater and meteoric water followed by meteoric water. Likely karst dissolution of fractures and other open space that were not filled by calcite cement. (f) Late Silurian and Devonian sea-level rise with deposition of the Woodford Shale (including the Misener Sandstone Member at its base). Siliciclastic infill of open-space pores in the Cochrane and Clarita Formations followed later by authigenic quartz, celestite, and saddle dolomite cement.

formed at near-surface temperatures (Gregg and Sibley, 1984; Sibley and Gregg, 1987).

Early diagenetic dolomitization by means of evaporated seawater (e.g., Adams and Rhodes, 1960; Hsü and Siegenthaler, 1969) is not likely in the Hunton Group carbonates in the study area as there is no evidence of evaporites or evaporated seawater during or soon after deposition. Further, $\delta^{18}O$ values for dolomites in the study area (table 3, fig. 12) fall close to values for calcites precipitated from Llandoverian and Wenlockian seawater (Azmy et al., 1998). More positive $\delta^{18}O$ values would be expected for dolomite precipitated from evaporated seawater (Land, 1980). Both the geological setting and isotope geochemistry indicate that dolomitization likely either occurred in a seawater or mixed fresh and seawater environment. A mixing zone dolomitization model (Folk and Land, 1975; Badiozamani, 1973) has been applied to dolomite in similar settings (e.g., Choquette and Steinen, 1980; Dunham and Olson, 1980; Humphrey and Quinn, 1989). Mixed water dolomitization was invoked for Hunton dolomites elsewhere in Oklahoma (Al-Shaieb et al., 2001). However, more recent work has highlighted the kinetic problems involved with nucleating dolomite crystals in brackish mixed water (Smart et al., 1988; Machel, 2004; see also Machel and Mountjoy, 1990), and this model for dolomitization has largely been abandoned (see Land, 1991).

Many earlier interpretations of important dolomite reservoirs and reservoir analogs that called on the mixing zone model of dolomitization (Folk and Land, 1975; Badiozamani, 1973) might better be reinterpreted using a normal seawater model (Saller, 1984). In that light, we invoke normal seawater as the likely dolomitizing fluid active in the Hunton Group carbonates in the study area (cf. Saller, 1984; Land, 1991). Reactive transport models demonstrate that movement of normal seawater by thermal convection through platform carbonates can lead to dolomitization of permeable carbonates (Whitaker et al., 2004; Whitaker and Xiao, 2010). In such models, complete dolomitization of a carbonate platform is possible within 10 to 15 m.y. at relatively low, near-surface temperatures (20 to 30°C) with relatively small geothermal gradients (Kahout, 1965; Whitaker and Xiao, 2010). Whitaker et al. (1994) use field evidence to show that such a mechanism may be applied to continuing dolomitization in the Great Bahama Bank beneath Andros Island. We speculate that a similar "Kahout" convection of normal seawater could have dolomitized the Hunton carbonates in the West Carney field area. Alternately, favorable marine currents may have been sufficient to drive seawater through the heavily karsted limestone, resulting in dolomitization (e.g., Land, 1991; Whitaker et al., 1994).

Distribution of dolomite in the WCHF study area does not follow any particular stratigraphic or lithological trends, and dolomitized sections are difficult, if not impossible, to correlate from core to core. This is especially the case in the Cochrane Formation, which is not as heavily dolomitized as the Clarita Formation. In the Cochrane Formation, the rather patchy occurrence of dolomite suggests that its distribution is controlled by porosity trends in this unit that in turn are the result of fracturing and karst dissolution of limestone during sea-level lowstands (fig. 13b). The cumulative dolomite thickness map shown in fig. 6b indicates a very irregular distribution of dolomite, consistent with a heavily karsted limestone and the resulting irregular permeability pathways during dolomitization. This distribution of dolomite, as well as the observation of more complete dolomitization of the Clarita Formation on the flanks of the carbonate buildup, favor a convective seawater model of dolomitization (fig. 13a and c) as described by Whitaker and Xiao (2010; see also fig. 14 in Amthor et al., 1993).

Petrographic differences between dolomite replacing the Cochrane and Clarita Formations may indicate separate timing of dolomitization. The difference in compositional zonation of the two dolomite types, revealed by CL microstratigraphy (fig. 11), may be due to Cochrane dolomite having been nucleated and beginning growth prior to dolomite in the Clarita. The slightly heavier $\delta^{13}C$ values of Clarita dolomite (fig. 12) may indicate the influence of organic methanogenic activity during precipitation of dolomite in the younger Clarita Formation or even a minor secular variation in $\delta^{13}C$ content of seawater between the time of Cochrane and Clarita dolomitization (Azmy et al., 1998).

Oxygen isotope values obtained for dolomite are problematic for a seawater interpretation of dolomitization. Dolomite precipitated in equilibrium with Llandoverian and Wenlockian seawater (fig. 12) at 25°C should display $\delta^{18}O$ values approximately 2 to 3‰ heavier than calcite due to the difference between the dolomite and calcite fractionation factor with water (Land, 1980). What is observed is that dolomite oxygen values largely overlap with or are only slightly heavier than Silurian seawater values (fig. 12). Part of this discrepancy may be due to warmer water (~30°C) that might be expected in a subtropical, restricted marine setting. A further shift toward lighter oxygen isotope values for dolomite may be due to alteration (dedolomitization) by mixed water and meteoric

water at the time of calcite cement precipitation. Many dolomite crystals display evidence of dedolomitization (fig. 11A), and this calcite likely was unavoidably included with dolomite sampled for isotope analysis.

Calcite Cements

Syn-sedimentary marine cements with characteristic radiaxial fibrous textures were not observed in Hunton limestones in the WCHF study area. Evidence exists for marine phreatic cementation, however, and is characterized by early (CL Z1) radial prismatic cement and syntaxial cement overgrowths on crinoid grains. This likely occurred in a reducing environment as evidenced by the non-CL response of the Z1 cement, indicating an elevated Fe^{2+} content, in the zone of microbial sulfate reduction (cf. Kaufman et al., 1988). This diagenetic environment also is indicated by light $\delta^{13}C$ values (fig. 12) (Hudson, 1977). Later calcite cements have an equant blocky texture, which is characteristic of the deeper phreatic environment. The CL microstratigraphy of calcite cements is not dissimilar to that of early burial phreatic cements in the overlying Mississippian of the midcontinent described by Kaufman et al. (1988), Mohammadi, Gregg et al. (2019), and Mohammadi, Ewald et al. (2019) and record redox variations in water chemistry.

The oxygen isotope values of CL Z1 and Z2 in the Cochrane Formation calcite cements mostly range from Wenlockian seawater values ($\delta^{18}O$ = -5.6 to -3.5‰) (Azmy et al., 1998) to somewhat lighter values ($\delta^{18}O$ = -7.8‰), indicating likely precipitation from seawater and/or a mixed seawater-meteoric water (table 2, fig. 12). Later Cochrane calcite cement (CL Z3) ranges in values from $\delta^{18}O$ = -7.87 to -2.27‰ (table 2, fig. 12). The heavier $\delta^{18}O$ values suggest precipitation from evaporated seawater. However, no evidence of evaporites were observed in the Hunton Group in the study area. Possibly periods of moderate evaporation may have existed during seawater lowstands or during the later Silurian or early Devonian. Any rocks deposited during these periods have been removed by subsequent erosion (fig. 2). Alternately, these heavier $\delta^{18}O$ values may reflect fluctuating chemistry of evolving basinal fluids. Most bulk calcite cement values from the Clarita Formation fall into the range expected for calcite precipitated from Wenlockian seawater or mixed seawater-meteoric water. One light outlier value ($\delta^{18}O$ = -9.59‰) (fig. 12) suggests the influence of hot basinal fluids (see discussion below).

The timing of calcite cementation can be determined through stratigraphic and petrographic relationships. There is no evidence of successive stages of calcite cementation with each sea-level rise and fall during deposition of the Cochrane and Clarita Formations (fig. 13). Such repeated cementation events would have been evidenced by a greater number of CL zones lower in the section, where limestones were exposed to more repeated sea-level changes than higher in the section. Rather, the pattern of CL zonation in calcite cements is consistent throughout the section. Petrographic evidence seems to indicate that most or all of the calcite cements postdate dolomitization. Most fractures, breccias, and associated siliciclastic infilling (fig. 10e–f) postdate calcite cement. The siliciclastic open-space-filling sediments likely were sourced from the overlying Misener Sandstone Member or the Woodford Shale higher in the section. Therefore, the evidence suggests that most calcite cementation occurred soon after dolomitization and prior to Misener-Woodford sedimentation (fig. 13d–f).

Late Diagenetic Events

Petrographic evidence documenting late diagenetic events in the WCHF study area is scarce. However, minor occurrence of open-space-filling saddle dolomite was observed in the Clarita Formation. Saddle dolomite is believed to precipitate at temperatures above 60°C (Radke and Mathis, 1980; Gregg and Sibley, 1984). Saddle dolomite cements have been observed in Hunton dolomites elsewhere in Oklahoma (Al-Shaieb et al., 2001). Significant late diagenetic alteration of Hunton carbonates, associated with deep burial, has been documented to the south of the study area in the Anadarko Basin (Friedman et al., 1984).

Open-space-filling authigenic quartz and celestite cements were observed near the base of the Hunton section in this study. Homogenization temperatures for fluid inclusion assemblages measured in celestite range from 131.2 to 285.7°C (table 1). However, given the wide range of T_h values within individual assemblages (Ray, 2018) and the propensity for fluid inclusions in celestite to stretch and neck down (Goldstein and Reynolds, 1994), only the lower range of temperatures are regarded as indicating actual filling temperatures. More reliable T_h values obtained for fluid inclusions in dolomite cements measured in the underlying Arbuckle Group range between 80 and 160°C (Temple et al., 2020). In the overlying Mississippian, T_h values in calcite cements range between 75 and 175°C (Mohammadi, Ewald et al., 2019). Salinities calculated from T_m measurements for fluid inclusion assemblages in Hunton celestite range from 16.1 to 22.4 equivalent weight % NaCl. These values fall within the range of salinities measured in the underlying Arbuckle dolomite cements

(Temple et al., 2020) and the higher range of salinities measured in the overlying Mississippian calcite cements (Mohammadi, Ewald et al., 2019). Therefore, the salinity values for the celestites are regarded as reliable. The Anadarko Basin to the south is thought to be the likely source of late diagenetic fluids in both the underlying Ordovician and overlying Mississippian carbonates (Temple et al., 2020; Mohammadi, Ewald et al., 2019). Expulsion of these fluids is believed to have taken place during the Pennsylvanian–Permian Ouachita orogeny via a regional gravity (topographical) flow system (Appold and Garven, 1999). Petroleum inclusions observed in the celestite crystals indicate that their precipitation was concurrent with petroleum generation and initial charging of the Hunton reservoir.

There is no evidence for significant late diagenetic alteration or recrystallization of dolomite (cf. Machel, 1997) in the WCHF study area during the migration of saline basinal fluids and emplacement of petroleum. Recrystallization of dolomite in the presence of warm (greater than 80°C) basinal fluids very likely would have shifted oxygen isotopes to significantly more negative values than those observed (fig. 12). Also, recrystallization of early diagenetic dolomite in the presence of basinal fluids typically results in coarse nonplanar crystal textures and homogenization of any compositional zoning (Gregg and Sibley, 1984; Gregg and Shelton, 1990; Machel, 1997). Neither of these textural alterations is displayed by dolomites observed replacing Hunton carbonates in this study. Thus, the replacive dolomite in the Silurian Cochrane and Clarita Formations in the West Carney Hunton oil field may represent an ancient example of early burial dolomitization by normal seawater that has been relatively unaltered by subsequent late diagenetic events.

CONCLUSIONS

Early diagenesis of the Cochrane and Clarita Formations in the West Carney Hunton Field (WCHF) in central Oklahoma was largely controlled by repeated Silurian sea-level fluctuations. Karst dissolution and early meteoric diagenesis of limestones occurred during sea-level lowstands. Partial to complete dolomitization of the limestones likely was a result of convective seawater circulation through the Hunton during sea-level highstands. The carbon and oxygen isotopic signatures of dolomite may have been partially reset by dedolomitization that took place during calcite cementation. Open-space-filling calcite cements postdate dolomitization and predate deposition of the overlying siliciclastic section comprising the Misener Sandstone and Woodford Shale. Carbon and oxygen isotope values for the calcite cements suggest precipitation by a range of fluids, including Silurian seawater and mixed seawater and meteoric water.

Analysis of included fluids in late diagenetic celestite crystals indicate that the WCHF was invaded by saline basinal fluids and petroleum after burial, probably during the Ouachita orogeny. There is no evidence that these late diagenetic fluids significantly altered the dolomite that formed earlier. The WCHF may provide an example of early diagenetic dolomitization by normal seawater that remains relatively unaltered by later diagenetic events.

ACKNOWLEDGMENTS

We thank John Chimahusky and Moe Nagaty at Equal Energy US Inc. for arranging financial support and Hunt Oil Co. for its financial support for this project. Marjo Operating Co., Inc. provided cores as well as the core analysis used in this study. We thank James Barrick for conodont identifications on 28 wells in the West Carney field. We thank Elliot Atekwana for his help with analysis and interpretation of isotope data. We also would like to thank Jackie Berryman, G. Michael Grammer, Sahar Mohammadi, Jack C. Pashin, James O. Puckette, Tracy Quan, Erin Roehrig, and the late Darwin R. Boardman II for their input and help with this project. Finally, we thank Stephen Kaczmarek and Abbas Seyedolali for their helpful reviews and Franek Hasiuk for his editorial handling of the manuscript.

REFERENCES

Adams, J. E., and Rhodes, M. L., 1960, Dolomitization by seepage refluxion: American AAPG Bulletin, v. 44, p. 1,912–1,920.

Al-Shaieb, Z., Puckette, J., and Blubaugh, P., 2001, The Hunton Group: Sequence stratigraphy, facies, dolomitization, and karstification; *in* Silurian, Devonian, and Mississippian geology and petroleum in the southern midcontinent, 1999 symposium, K. S. Johnson, ed.: Oklahoma Geological Survey Circular 105, p. 17–29.

Amsden, T. W., and Rowland, T. L., 1971, Silurian and Lower Devonian (Hunton) oil- and gas-producing formations: AAPG Bulletin, v. 55, p. 104–109.

Amthor, J. E., Mountjoy, E. W., and Machel, H. G., 1993, Subsurface dolomites in Upper Devonian Leduc Formation buildups, central part of Rimbey-Meadowbrook reef trend, Alberta, Canada: Bulletin of Canadian Petroleum Geology, v. 41, p. 164–185.

Appold, M. S., and Garven, G., 1999, The hydrology of ore formation in the Southeast Missouri District: Numerical models of topography-driven fluid flow during the Ouachita Orogeny: Economic Geology, v. 94, p. 913–936.

Azmy, K., Veizer, J., Bassett, M. G., and Copper, P., 1998, Oxygen and carbon isotopic composition of Silurian brachiopods: Implications for coeval seawater and glaciations: GSA Bulletin, v. 110, p. 1,499–1,512.

Bader, J. D., 2007, Telychian (Llandovery, Silurian) conodonts from the Chimneyhill Subgroup, West Carney Hunton Field, north-central Oklahoma: M.S. thesis, Texas Tech University, 83 p.

Bader, J. D., Barrick, J. E., and Derby, J. R., 2007, Telychian (Llandovery, Silurian) conodonts from a new stratigraphic unit in the Chimneyhill Subgroup, West Carney Hunton Field, North-Central Oklahoma: South-Central/North-Central Section: Geologic Society of America Abstracts with Programs, v. 39, no. 3, p. 62.

Badiozamani, K., 1973, The dorag dolomitization model — Application to the Middle Ordovician of Wisconsin: Journal of Sedimentary Petrology, v. 43, p. 965–984.

Bathurst, R. G. C., 1975, Carbonate Sediments and Their Diagenesis: New York, Elsevier Scientific Publishing Co., 658 p.

Bodner, R. J., 1993, Revised equation and table for determining the freezing point depression of H20-NaCl solutions: Geochimica et Cosmochimica Acta, v. 57, p. 683–684.

Braimoh, K. A., 2010, Deepwater, shoalwater, and lagoonal facies in the Silurian Upper Cochrane member, Hunton Group, Chimney Hill Subgroup, West Carney Hunton field, Oklahoma: M.S. thesis, University of Tulsa, 190 p.

Choquette, P. W., and Pray, L. C., 1970, Geologic nomenclature and classification of porosity in sedimentary carbonates: AAPG Bulletin, v. 54, p. 207–250.

Choquette, P. W., and Steinen, R. P., 1980, Mississippi nonsupratidal dolomite, Ste Genevieve Limestone, Illinois Basin: Evidence for mixed water dolomitization; *in* Concepts and Models of Dolomitization, D. H. Zenger, J. B. Dunham, and R. L. Ethington, eds.: SEPM, Special Publication 28, p. 168–196.

Derby, J. R., 2007, Geologic studies of West Carney Hunton Field; in Exploitation and optimization of reservoir performance in Hunton Formation, Oklahoma — Final technical report, University of Tulsa, Department of Petroleum Engineering, DOE Contract No. DE FC26-00NT15125, U.S. Department of Energy, August 27 of 2007, M. Kelkar, ed.: University of Tulsa, p. 42–65.

Derby, J. R., Podpechan, F. J., Andrews, J., and Ramakrishna, S., 2002a, U.S. DOE-sponsored study of West Carney Hunton Field, Lincoln & Logan counties, Oklahoma: A preliminary report (Part I): Shale Shaker, v. 52, p. 9–19.

Derby, J. R., Podpechan, F. J., Andrews, J., and Ramakrishna, S., 2002b, U.S. DOE-sponsored study of West Carney Hunton Field, Lincoln & Logan counties, Oklahoma: A preliminary report (Part II Conclusion): Shale Shaker, v. 52, p. 39–48.

Dunham, J. B., and Olson, E. R., 1980, Shallow subsurface dolomitization of subtidally deposited carbonate sediments in the Hanson Creek Formation (Ordovician-Silurian) of central Nevada; *in* Concepts and models of dolomitization, D. H. Zenger, J. B. Dunham, and R. L. Ethington, eds.: SEPM, Special Publication 28, p. 139–161.

Dunham, R. J., 1962, Classification of carbonate rocks according to depositional texture; *in* Classification of carbonate rocks, W. E. Ham, ed.: AAPG, Memoir 1, p. 108–121.

Folk, R. L., 1959, Practical petrographic classification of limestones: AAPG Bulletin, v. 43, no. 1, p. 1–38.

Folk, R. L., and Land, L. S., 1975, Mg/Ca ratio and salinity: Two controls over crystallization of dolomite: AAPG Bulletin, v. 56, p. 434–453.

Friedman, G. M., 1959, Identification of carbonate minerals by staining methods: Journal of Sedimentary Petrology, v. 29, no. 1, p. 87–97.

Friedman, G. M., Cattafe, J., and Borak, B., 1984, Deep-burial diagenesis of the Hunton (Late Ordovician to Early Devonian) carbonates in the Anadarko Basin; *in* Limestones of the Mid-continent, N. J. Hyne, ed.: Tulsa Geological Society, Special Publication no. 2, p. 183–199.

Goldstein, R. H., and Reynolds, T. J., 1994, Systematics of fluid inclusions in diagenetic minerals: Tulsa, Oklahoma, SEPM, Short Course 31, 199 p. doi: 10.2110/scn.94.31

Gregg, J. M., Bish, D. L., Kaczmarek, S. E., and Machel, H. G., 2015, Mineralogy, nucleation and growth of dolomite in the laboratory and sedimentary environment: A review: Sedimentology, v. 62, p. 1,749–1,769. doi: 10.1111/sed.12202

Gregg, J. M., and Shelton, K. L., 1990, Dolomitization and dolomite neomorphism in the back reef facies of the Bonneterre and Davis Formations (Cambrian), southeast Missouri: Journal of Sedimentary Petrology, v. 60, p. 549–562.

Gregg, J. M., and Sibley, D. F., 1984, Epigenetic dolomitization and the origin of xenotopic dolomite texture: Journal of Sedimentary Petrology, v. 54, p. 908–931.

Hsü, K. J., and Siegenthaler, C., 1969, Preliminary experiments on hydrodynamic movement induced by evaporation and their bearing on the dolomite problem: Sedimentology, v. 12, p. 11–25.

Hudson, J. D., 1977, Stable isotopes and limestone lithification: Journal of the Geological Society London, v. 133, p. 637–660.

Humphrey, J. D., and Quinn, T. M., 1989, Coastal mixing zone dolomite, forward modeling, and massive dolomitization of platform-margin carbonates: Journal of Sedimentary Petrology, v. 59, p. 438–454.

Johnson, M. E., 1987, Extent and bathymetry of North American platform seas in the Early Silurian: Paleoceanography, v. 2, p. 184–211.

Johnson, M. E., 2006, Relationship of Silurian sea level fluctuations to oceanic episodes and events: GFF (Geologiska Föreningen i Stockholm Förhandlingar), v. 128, p. 115–121.

Kahout, F. A., 1965, A hypothesis concerning cyclic flow of salt water related to geothermal heating in the Floridan aquifer: Transactions of the New York Academy of Sciences, v. 28, p. 249–271.

Kaufman, J., Cander, H. S., Daniels, L. D., and Meyers, W. J., 1988, Calcite cement stratigraphy and cementation history of the Burlington-Keokuk Formation (Mississippian), Illinois and Missouri: Journal of Sedimentary Petrology, v. 58, p. 312–326.

Krishnamurthy, R. V., Atekwana, E. A., and Guha, H., 1997, A simple, inexpensive carbonate–phosphoric acid reaction method for the analysis of carbon and oxygen isotopes of carbonates: Analytical Chemistry, v. 69, p. 4,256–4,258.

Land, L. S., 1980, The isotopic and trace element geochemistry of dolomite: The state of the art; *in* Concepts and models of dolomitization, D. H. Zenger, J. B. Dunham, and R L. Ethington, eds.: SEPM, Special Publication 28, p. 87–110.

Land, L. S., 1991, Dolomitization of the Hope Gate Formation (north Jamaica) by seawater: Reassessment of mixing-zone dolomite; *in* Stable isotope geochemistry: A tribute to Samuel Epstein, H. P. Taylor, Jr., J. R. O'Neil, and I. R. Kaplan, eds.: The Geochemical Society, Special Publication 3, p. 121–133.

Lumsden, D. N., 1979, Discrepancy between thin-section and X-ray estimates of dolomite in limestone: Journal of Sedimentary Petrology, v. 49, p. 429–436.

Machel, H. G., 1997, Recrystallization verses neomorphism, and the concept of "significant recrystallization" in dolomite research: Sedimentary Geology, v. 113, p. 161–168.

Machel, H. G., 2004, Concepts and models of dolomitization — a critical reappraisal; *in* The geometry and petrogenesis of dolomite hydrocarbon reservoirs, C. J. R. Braithwaite, G. Rizzi, and G. Darke, eds.: Geological Society London, Special Publication 235, p. 7–63.

Machel, H. G., and Mountjoy, E. W., 1990, Coastal mixing zone dolomite, forward modeling, and massive dolomitization of platform-margin carbonates — discussion: Journal of Sedimentary Petrology, v. 60, no. 6, p. 1,008–1,012.

Mohammadi, S., Ewald, T., Gregg, J. M., and Shelton, K. L., 2019, Diagenetic history of Mississippian carbonate rocks in the Nemaha Ridge area, north-central Oklahoma, USA; *in* Mississippian reservoirs of the midcontinent, G. M. Grammer, J. G. Gregg, J. Puckette, P. Jaiswal, S. J. Mazzullo, M. J. Pranter, and R. H. Goldstein, eds: Tulsa, Oklahoma, AAPG Memoir 122, p. 323–352. DOI:10.1306/13632153M1163791

Mohammadi, S., Gregg, J. M., Shelton, K. L., Appold, M. S., and Puckette, J. O., 2019, Influence of late diagenetic fluids on Mississippian carbonate rocks on the Cherokee–Ozark Platform, NE Oklahoma, NW Arkansas, SW Missouri, and SE Kansas; *in* Mississippian reservoirs of the midcontinent, G. M. Grammer, J. G. Gregg, J. Puckette, P. Jaiswal, S. J. Mazzullo, M. J. Pranter, and R. H. Goldstein, eds: Tulsa, Oklahoma, AAPG Memoir 122, p. 353–378. DOI:10.1306/13632154M1163791

Radke, B. M., and Mathis, R. L., 1980, On the formation and occurrence of saddle dolomite: Journal of Sedimentary Petrology, v. 50, p. 1,149–1,168.

Ray, J. T., 2018, Reservoir and diagenetic characteristics of the Clarita Formation, Hunton Group — Lincoln and Logan Counties, Oklahoma: M.S. thesis, Oklahoma State University, 64 p.

Saller, A. H., 1984, Petrologic and geochemical constraints on the origin of subsurface dolomite, Eniwetak Atoll: An example of dolomitization by normal seawater: Geology, v. 12, p. 217–220.

Scotese, C. R., 2002, PALEOMAP Project: http://www.scotese.com/newpage2.htm.

Scotese, C. R., and McKerrow, W. S., 1990, Revised world maps and introduction; *in* Palaeozoic palaeogeography and biogeography, W.S. McKerrow and C. R. Scotese, ed.: Geological Society London, Memoir 12, p. 1–21.

Sibley, D. F., and Gregg, J. M., 1987, Classification of dolomite rock textures: Journal of Sedimentary Petrology, v. 57, p. 967–975.

Silva, C., 2012, Reservoir and diagenetic characterization of the Lower Cochrane Member, Hunton Group — Lincoln and Logan Counties: M.S. thesis, Oklahoma State University, 64 p.

Smart, P. L., Dawans, J. M., and Whitaker, F., 1988, Carbonate dissolution in a modern mixing zone: Nature, v. 335, p. 811–813.

Smith, B. J., 2012, Effects of sea level fluctuations on porosity and permeability of the lower Cochrane member, Chimneyhill Subgroup, Hunton Group West Carney Hunton Field Logan County, OK: M.S. thesis, Oklahoma State University, 80 p.

Temple, B. J., Bailey, P. A., and Gregg, J. M., 2020, Carbonate diagenesis of the Arbuckle Group north central Oklahoma to Southeastern Missouri: Shale Shaker, v. 70, p. 248–267.

Whitaker, F. F., Smart, P. L., and Jones, G. D., 2004, Dolomitization: From conceptual to numerical models; *in* The geometry and petrogenesis of dolomite hydrocarbon reservoirs, C. J. R. Braithwaite, G. Rizzi, and G. Darke, eds.: Geological Society London, Special Publication 235, p. 99–139.

Whitaker, F. F., Smart, P. L., Vahrenkamp, V. C., Nicholson, H., and Wogelius, R. A., 1994, Dolomitization by near-normal seawater? Field evidence from the Bahamas; *in* Dolomites A volume in honor of Dolomieu, B. Purser, M. Tucker, and D. Zenger, eds.: International Association of Sedimentologists, Special Publication 21, p. 111–132.

Whitaker, F. F., and Xiao, Y., 2010, Reactive transport modeling of early burial dolomitization of carbonate platforms by geothermal convection: AAPG Bulletin, v. 94, p. 889–917. DOI:10.1306/12090909075

Midcontinent Geoscience • Volume 1 • September 2020
Tony Layzell – Editor
Section Editor — Franek Hasiuk
Technical Editor — Julie Tollefson

Suggested citation: Silva, C., Smith, B. J., Ray, J. T., Derby, J. R., and Gregg, J. M., 2020, Diagenesis of Hunton Group carbonates (Silurian) West Carney Field, Logan and Lincoln counties, Oklahoma, U.S.A.: Midcontinent Geoscience, v. 1, p. 30–51.

Midcontinent Geoscience is an open-access, peer-reviewed journal of the Kansas Geological Survey. The journal publishes original research on a broad array of geoscience topics, with an emphasis on the midcontinent region of the United States, including the Great Plains and Central Lowland provinces.

Submission information: https://journals.ku.edu/mg/about/submissions

Kansas Geological Survey
1930 Constant Avenue
The University of Kansas
Lawrence, KS 66047-3724
785.864.3965

http://www.kgs.ku.edu/

KU
KANSAS
GEOLOGICAL
SURVEY
The University of Kansas